Appendix

Table of Contents

A Proof

A.1 Proof of Theorem 1

Theorem 1. *We have $\Delta_{dp}(\hat{Y}, S)$ and $W(\hat{Y}, S)$ upper bounded by $TV(\hat{Y}, S)$. Moreover, $I(\hat{Y}, S)$ is also upper bounded by $TV(\hat{Y}, S)$ if $\forall z \in [0,1]$, $P_{\hat{Y}}(z) \geq \Pi_i \Pr(S=i)$ holds.*

Proof. $\Delta_{dp}(\hat{Y}, S)$, $I(\hat{Y}, S)$, $W(\hat{Y}, S)$, and $TV(\hat{Y}, S)$ are all non-negative. We first prove that $\Delta_{dp}(\hat{Y}, S)$ is upper bounded by $TV(\hat{Y}, S)$. Recall that $TV(\hat{Y}, S) = \int_0^1 |P_{\hat{Y}|S=0}(z) - P_{\hat{Y}|S=1}(z)| dz$, we have

$$\begin{aligned}
\Delta_{dp}(\hat{Y}, S) =& \left| \Pr\left(\hat{Y} \geq \frac{1}{2} \mid S=0\right) - \Pr\left(\hat{Y} \geq \frac{1}{2} \mid S=1\right) \right| \\
=& \left| \int_{\frac{1}{2}}^1 P_{\hat{Y}|S=0}(z) - P_{\hat{Y}|S=1}(z) dz \right| \\
\leq& \int_{\frac{1}{2}}^1 \left| P_{\hat{Y}|S=0}(z) - P_{\hat{Y}|S=1}(z) \right| dz \\
\leq& \int_0^1 \left| P_{\hat{Y}|S=0}(z) - P_{\hat{Y}|S=1}(z) \right| dz \\
=& TV(\hat{Y}, S).
\end{aligned}$$

Next, we prove that $W(\hat{Y}, S)$ is also upper bounded by $TV(\hat{Y}, S)$.

$$\begin{aligned}
W(\hat{Y}, S) &= \int_0^1 \left| F^{-1}_{\hat{Y}|S=0}(y) - F^{-1}_{\hat{Y}|S=1}(y) \right| dy \\
&= \int_0^1 \left| F_{\hat{Y}|S=0}(z) - F_{\hat{Y}|S=1}(z) \right| dz.
\end{aligned} \tag{6}$$

This equation holds because we know that $F_{\hat{Y}|S=0}(0) = F_{\hat{Y}|S=1}(0) = 0$ and $F_{\hat{Y}|S=0}(1) = F_{\hat{Y}|S=1}(1) = 1$ according to the property of cumulative distribution function and the fact that $\hat{Y} \in [0,1]$. Hence $y = F_{\hat{Y}|S=0}(z)$ and $y = F_{\hat{Y}|S=1}(z)$ form a closed curve in $[0,1] \times [0,1]$ in z-y plane. Consequently, Equation (6) could be seen as computing the area of the closed curve from the y-axis and z-axis separately. Consequently, we have

$$\begin{aligned}
W(\hat{Y}, S) =& \int_0^1 \left| F_{\hat{Y}|S=0}(z) - F_{\hat{Y}|S=1}(z) \right| dz \\
=& \int_0^1 \left| \int_0^x P_{\hat{Y}|S=0}(z) dz - \int_0^x P_{\hat{Y}|S=1}(z) dz \right| dx \\
\leq& \int_0^1 \int_0^x \left| P_{\hat{Y}|S=0}(z) dz - P_{\hat{Y}|S=1}(z) \right| dz dx \\
=& \int_0^{x'} \left| P_{\hat{Y}|S=0}(z) dz - P_{\hat{Y}|S=1}(z) \right| dz, \ x' \in [0,1] \\
\leq& \int_0^1 \left| P_{\hat{Y}|S=0}(z) dz - P_{\hat{Y}|S=1}(z) \right| dz \\
=& TV(\hat{Y}, S).
\end{aligned}$$

Finally, we prove that $I(\hat{Y}, S)$ is upper bounded by $TV(\hat{Y}, S)$ if $\forall z \in [0,1]$, $P_{\hat{Y}}(z) \geq \Pi_i \Pr(S=i)$. First, we have

$$I(\hat{Y}, S) = \int_0^1 \sum_i P_{\hat{Y},S}(z,i) \log \frac{P_{\hat{Y},S}(z,i)}{P_{\hat{Y}}(z) \Pr(S=i)} dz$$

$$= \int_0^1 \sum_i \Pr(S=i) P_{\hat{Y}|S=i}(z) \log \frac{P_{\hat{Y}|S=i}(z)}{P_{\hat{Y}}(z)} dz.$$

Let $P_i = \Pr(S=i)$ for $i=0,1$, then we have $P_0 + P_1 = 1$ and $P_{\hat{Y}}(z) = P_0 P_{\hat{Y}|S=0}(z) + P_1 P_{\hat{Y}|S=1}(z)$. According to the fact that $\log x \leq x-1$ for $x \in (0,1]$, we let $x = \frac{P_{\hat{Y}|S=i}(z)}{P_{\hat{Y}}(z)}$ and have

$$\begin{aligned}
I(\hat{Y},S) &= \int_0^1 \sum_i P_i P_{\hat{Y}|S=i}(z) \log \frac{P_{\hat{Y}|S=i}(z)}{P_{\hat{Y}}(z)} dz \\
&\leq \int_0^1 \sum_i P_i \frac{\left(P_{\hat{Y}|S=i}(z)\right)^2}{P_{\hat{Y}}(z)} - P_i P_{\hat{Y}|S=i}(z) dz \\
&= \int_0^1 \sum_i P_i \frac{P_{\hat{Y}|S=i}(z)\left(P_{\hat{Y}|S=i}(z) - P_{\hat{Y}}(z)\right)}{P_{\hat{Y}}(z)} dz \\
&= \int_0^1 \frac{P_0 P_1 P_{\hat{Y}|S=0}(z)\left(P_{\hat{Y}|S=0}(z) - P_{\hat{Y}|S=1}(z)\right)}{P_0 P_{\hat{Y}|S=0}(z) + P_1 P_{\hat{Y}|S=1}(z)} \\
&\quad + \frac{P_0 P_1 P_{\hat{Y}|S=1}(z)\left(P_{\hat{Y}|S=1}(z) - P_{\hat{Y}|S=0}(z)\right)}{P_0 P_{\hat{Y}|S=0}(z) + P_1 P_{\hat{Y}|S=1}(z)} dz \\
&= \int_0^1 \frac{P_0 P_1 \left(P_{\hat{Y}|S=0}(z) - P_{\hat{Y}|S=1}(z)\right)^2}{P_0 P_{\hat{Y}|S=0}(z) + P_1 P_{\hat{Y}|S=1}(z)} dz.
\end{aligned} \tag{7}$$

Given that $P_{\hat{Y}}(z) \geq \Pi_i \Pr(S=i)\ \forall z \in [0,1]$, we have $P_0 P_{\hat{Y}|S=0}(z) + P_1 P_{\hat{Y}|S=1}(z) \geq P_0 P_1 (P_0 + P_1) = P_0 P_1$. Consequently, we have

$$I(\hat{Y},S) \leq \int_0^1 \left(P_{\hat{Y}|S=0}(z) - P_{\hat{Y}|S=1}(z)\right)^2 dz.$$

Considering that the training of fairness-aware GNNs makes the distributions $P_{\hat{Y}|S=0}(z)$ and $P_{\hat{Y}|S=1}(z)$ closer, we assume that $|P_{\hat{Y}|S=0}(z) - P_{\hat{Y}|S=1}(z)| \leq 1$ for $z \in [0,1]$. To verify this assumption, we conduct numerical experiments on all three adopted datasets. Following our methodology, we use the kernel density estimation to estimate the distribution functions $P_{\hat{Y}|S=0}(z)$ and $P_{\hat{Y}|S=1}(z)$ and compute the value of $|P_{\hat{Y}|S=0}(z) - P_{\hat{Y}|S=1}(z)|$ consequently. We record the largest value of $|P_{\hat{Y}|S=0}(z) - P_{\hat{Y}|S=1}(z)|$ for $z \in [0,1]$ and obtain the results as 0.1372 ± 0.0425 for Facebook, 0.0999 ± 0.0310 for Pokec_z, and 0.0356 ± 0.0074 for Credit (mean value and standard deviation under 5 random seeds), which are all far less than 1. Then, we come to

$$I(\hat{Y},S) \leq \int_0^1 \left| P_{\hat{Y}|S=0}(z) - P_{\hat{Y}|S=1}(z) \right| dz = TV(\hat{Y},S). \tag{8}$$

In conclusion, we have proved that $\Delta_{dp}(\hat{Y},S)$ and $W(\hat{Y},S)$ are upper bounded by $TV(\hat{Y},S)$. Moreover, $I(\hat{Y},S)$ is also upper bounded by $TV(\hat{Y},S)$ if $\forall z \in [0,1]$, $P_{\hat{Y}}(z) \geq \Pi_i \Pr(S=i)$ holds.

$\square$

Remarks on Theorem 1. It is worth noting that $I(\hat{Y},S) \leq TV(\hat{Y},S)$ stems from the condition of $P_{\hat{Y}}(z) \geq \Pi_i \Pr(S=i), \forall z \in [0,1]$. Although we are not able to always ensure the correctness of the condition in practice, we can still obtain from Theorem 1 that (1) the probability of the condition holds grows larger when the number of sensitive groups increases; (2) even in the binary case, the condition is highly likely to hold in practice, considering that $\Pr(S=0) \cdot \Pr(S=1) \leq \frac{1}{4}$ (In a binary case, we have $\Pr(s=0) + \Pr(s=1) = 1$; hence, $\Pr(s=0)\Pr(s=1) = \Pr(s=0)(1-\Pr(s=0)) \leq 1/4$).

To further improve the soundness of our theoretical analysis, we can slightly loosen the condition $P_{\hat{Y}}(z) \geq \Pi_i \Pr(S = i)\ \forall z \in [0, 1]$ and obtain a new condition $\int_0^1 \left(\frac{P_0 P_1}{P_0 P_{\hat{Y}|S=0}(z) + P_1 P_{\hat{Y}|S=1}(z)} \right)^2 dz \leq 1$. Consider the last step of Equation (7). According to the Cauchy-Schwartz inequality, we have

$$
\begin{aligned}
I(\hat{Y}, S) &\leq \int_0^1 \frac{P_0 P_1 \left(P_{\hat{Y}|S=0}(z) - P_{\hat{Y}|S=1}(z) \right)^2}{P_0 P_{\hat{Y}|S=0}(z) + P_1 P_{\hat{Y}|S=1}(z)} dz \\
&\leq \left(\int_0^1 \left(\frac{P_0 P_1}{P_0 P_{\hat{Y}|S=0}(z) + P_1 P_{\hat{Y}|S=1}(z)} \right)^2 dz \cdot \int_0^1 \left(P_{\hat{Y}|S=0}(z) - P_{\hat{Y}|S=1}(z) \right)^4 dz \right)^{\frac{1}{2}} \\
&\leq \left(\int_0^1 \left(P_{\hat{Y}|S=0}(z) - P_{\hat{Y}|S=1}(z) \right)^4 dz \right)^{\frac{1}{2}} \\
&\leq \sqrt{TV(\hat{Y}, S)}.
\end{aligned}
$$

Consequently, we obtain a variant of Theorem 1 as follows.

Theorem A 1. *$I(\hat{Y}, S)$ is upper bounded by $\sqrt{TV(\hat{Y}, S)}$, if $\int_0^1 \left(\frac{P_0 P_1}{P_0 P_{\hat{Y}|S=0}(z) + P_1 P_{\hat{Y}|S=1}(z)} \right)^2 dz \leq 1$ holds.*

According to Theorem A 1, we find a looser upper bound for $I(\hat{Y}, S)$ (still dependent on $TV(\hat{Y}, S)$) based on a weaker condition. In addition, Theorem A 1 is able to support our total variation loss as well, since we still have $I(\hat{Y}, S)$ approaches 0 when $TV(\hat{Y}, S)$ approaches 0 after training. Similar as the assumption $|P_{\hat{Y}|S=0}(z) - P_{\hat{Y}|S=1}(z)| \leq 1$, we conduct numerical experiments with kernel density estimation for estimating $P_{\hat{Y}|S=0}(z)$ and $P_{\hat{Y}|S=1}(z)$ and numerical integral for computing the value of $\int_0^1 \left(\frac{P_0 P_1}{P_0 P_{\hat{Y}|S=0}(z) + P_1 P_{\hat{Y}|S=1}(z)} \right)^2 dz$. We obtain the results of the integral as 0.8621 ± 0.1110 for Facebook, 0.4568 ± 0.0666 for Pokec_z, and 0.5934 ± 0.0763 for Credit (mean value and standard deviation under 5 random seeds). Experimental results verify the feasibility of the condition in Theorem A 1.

A.2 PROOF OF THEOREM 2

Theorem 2. *The optimal poisoned adjacency matrix $\mathbf{A}^{t+1}$ in the $t+1$-th iteration given by PGD, i.e., the solution of $\mathbf{A}^{t+1} = \operatorname{argmin}_{|\mathcal{L}(\mathbf{A}^t) - \mathcal{L}(\mathbf{A}')| \leq \epsilon_t} \|\mathbf{A}' - (\mathbf{A}^t + \eta \nabla \mathcal{L}_f(\mathbf{A}^t))\|_F^2$ is*

$$
\mathbf{A}^{t+1} = \begin{cases} \mathbf{A}^t + \eta \nabla_{\mathbf{A}} \mathcal{L}_f(\mathbf{A}^t), \ \textit{if}\ \eta |\nabla_{\mathbf{A}} \mathcal{L}(\mathbf{A}^t)^T \nabla_{\mathbf{A}} \mathcal{L}_f(\mathbf{A}^t)| \leq \epsilon_t, \\ \mathbf{A}^t + \eta \nabla_{\mathbf{A}} \mathcal{L}_f(\mathbf{A}^t) + \dfrac{e_t \epsilon_t - \eta \nabla_{\mathbf{A}} \mathcal{L}(\mathbf{A}^t)^T \nabla_{\mathbf{A}} \mathcal{L}_f(\mathbf{A}^t)}{\|\nabla_{\mathbf{A}} \mathcal{L}(\mathbf{A}^t)\|_F^2} \nabla_{\mathbf{A}} \mathcal{L}(\mathbf{A}^t), \ \textit{otherwise}, \end{cases} \tag{9}
$$

where $e_t = \operatorname{sign}\left(\nabla_{\mathbf{A}} \mathcal{L}(\mathbf{A}^t)^T \nabla_{\mathbf{A}} \mathcal{L}_f(\mathbf{A}^t) \right)$.

Proof. First, we know that $\mathbf{A}' = \mathbf{A}^t$ is a feasible solution because $\mathcal{L}(\mathbf{A}^t) - \mathcal{L}(\mathbf{A}^t) = 0 \leq \epsilon_t$. Hence we assume that $\mathbf{A}'$ is close to $\mathbf{A}^t$. Consequently, we use the first-order Taylor expansion to substitute the constraint $|\mathcal{L}(\mathbf{A}') - \mathcal{L}(\mathbf{A}^t)| \leq \epsilon_t$ as $\left| \nabla \mathcal{L}(\mathbf{A}^t)^T (\mathbf{A}' - \mathbf{A}^t) \right| \leq \epsilon_t$. For simplicity, we vectorize the adjacency matrices $\mathbf{A}^t$ and $\mathbf{A}'$ here such that $\mathbf{A}^t, \mathbf{A}' \in \mathbb{R}^{n^2}$.

Next, we let $\mathbf{A}' = \mathbf{A}^t + \eta \nabla \mathcal{L}_f(\mathbf{A}^t) + \boldsymbol{\xi}$, and convert the optimization problem as follows.

$$
\mathbf{A}^{t+1} = \operatorname*{argmin}_{|\nabla \mathcal{L}(\mathbf{A}^t)^T (\eta \nabla \mathcal{L}_f(\mathbf{A}^t) + \boldsymbol{\xi})| \leq \epsilon_t} \|\boldsymbol{\xi}\|_2^2. \tag{10}
$$

Then we discuss the new constraint in Equation (10) $|\eta \nabla \mathcal{L}(\mathbf{A}^t)^T \nabla \mathcal{L}_f(\mathbf{A}^t) + \nabla \mathcal{L}(\mathbf{A}^t)^T \boldsymbol{\xi}| \leq \epsilon_t$ in different conditions.

(1). When $|\eta \nabla \mathcal{L}(\mathbf{A}^t)^T \nabla \mathcal{L}_f(\mathbf{A}^t)| \leq \epsilon_t$, we can easily obtain the optimal solution as $\boldsymbol{\xi} = \mathbf{0}$.

(2). When $\eta \nabla \mathcal{L}(\mathbf{A}^t)^T \nabla \mathcal{L}_f(\mathbf{A}^t) \geq \epsilon_t$, then we have

$$-\epsilon_t - \eta \nabla \mathcal{L}(\mathbf{A}^t)^T \nabla \mathcal{L}_f(\mathbf{A}^t) \leq \nabla \mathcal{L}(\mathbf{A}^t)^T \boldsymbol{\xi} \leq \epsilon_t - \eta \nabla \mathcal{L}(\mathbf{A}^t)^T \nabla \mathcal{L}_f(\mathbf{A}^t).$$

Because $\nabla \mathcal{L}(\mathbf{A}^t)^T \boldsymbol{\xi} = \|\nabla \mathcal{L}(\mathbf{A}^t)\|_2 \cdot \|\boldsymbol{\xi}\|_2 \cdot \cos\theta$, where θ is the angle of $\nabla \mathcal{L}(\mathbf{A}^t)$ and $\boldsymbol{\xi}$. To minimize $\|\boldsymbol{\xi}\|_2$, we minimize $\cos\theta$ as $\cos\theta = -1$, i.e., $\boldsymbol{\xi} = -\|\boldsymbol{\xi}\|_2 \cdot \nabla \mathcal{L}(\mathbf{A}^t)/\|\nabla \mathcal{L}(\mathbf{A}^t)\|_2$, and then have

$$\frac{-\epsilon_t + \eta \nabla \mathcal{L}(\mathbf{A}^t)^T \nabla \mathcal{L}_f(\mathbf{A}^t)}{\|\nabla \mathcal{L}(\mathbf{A}^t)\|_2} \leq \|\boldsymbol{\xi}\|_2 \leq \frac{\epsilon_t + \eta \nabla \mathcal{L}(\mathbf{A}^t)^T \nabla \mathcal{L}_f(\mathbf{A}^t)}{\|\nabla \mathcal{L}(\mathbf{A}^t)\|_2}.$$

Therefore, the solution of Equation (10) is

$$\boldsymbol{\xi} = \frac{\epsilon_t - \eta \nabla \mathcal{L}(\mathbf{A}^t)^T \nabla \mathcal{L}_f(\mathbf{A}^t)}{\|\nabla \mathcal{L}(\mathbf{A}^t)\|_2^2} \nabla \mathcal{L}(\mathbf{A}^t).$$

(3). When $\eta \nabla \mathcal{L}(\mathbf{A}^t)^T \nabla \mathcal{L}_f(\mathbf{A}^t) \leq -\epsilon_t$, we also have

$$-\epsilon_t - \eta \nabla \mathcal{L}(\mathbf{A}^t)^T \nabla \mathcal{L}_f(\mathbf{A}^t) \leq \nabla \mathcal{L}(\mathbf{A}^t)^T \boldsymbol{\xi} \leq \epsilon_t - \eta \nabla \mathcal{L}(\mathbf{A}^t)^T \nabla \mathcal{L}_f(\mathbf{A}^t).$$

Different from condition (2), the left-hand side and right-hand side here are both positive. Similarly, we let $\cos\theta = 1$ and obtain the solution of Equation (10) as

$$\boldsymbol{\xi} = \frac{-\epsilon_t - \eta \nabla \mathcal{L}(\mathbf{A}^t)^T \nabla \mathcal{L}_f(\mathbf{A}^t)}{\|\nabla \mathcal{L}(\mathbf{A}^t)\|_2^2} \nabla \mathcal{L}(\mathbf{A}^t).$$

Combine the aforementioned three conditions into $\mathbf{A}' = \mathbf{A}^t + \eta \nabla \mathcal{L}_f(\mathbf{A}^t) + \boldsymbol{\xi}$, then we have the solution as follows

$$\mathbf{A}^{t+1} = \begin{cases} \mathbf{A}^t + \eta \nabla_{\mathbf{A}} \mathcal{L}_f(\mathbf{A}^t), \ \textbf{if} \ \eta |\nabla_{\mathbf{A}} \mathcal{L}(\mathbf{A}^t)^T \nabla_{\mathbf{A}} \mathcal{L}_f(\mathbf{A}^t)| \leq \epsilon_t, \\ \mathbf{A}^t + \eta \nabla_{\mathbf{A}} \mathcal{L}_f(\mathbf{A}^t) + \dfrac{e_t \epsilon_t - \eta \nabla_{\mathbf{A}} \mathcal{L}(\mathbf{A}^t)^T \nabla_{\mathbf{A}} \mathcal{L}_f(\mathbf{A}^t)}{\|\nabla_{\mathbf{A}} \mathcal{L}(\mathbf{A}^t)\|_F^2} \nabla_{\mathbf{A}} \mathcal{L}(\mathbf{A}^t), \ \text{otherwise}, \end{cases}$$

where $e_t = \text{sign}\left(\nabla_{\mathbf{A}} \mathcal{L}(\mathbf{A}^t)^T \nabla_{\mathbf{A}} \mathcal{L}_f(\mathbf{A}^t)\right)$. □

B ATTACK SETTINGS

In this section, we introduce our attack settings in detail from three perspectives, the attacker's goal, the attacker's knowledge, and the attacker's capability.

Attacker's Goal. There are two different settings of our problem, the fairness evasion attack, and the fairness poisoning attack. In the fairness evasion attack, the attacker's goal is to let the victim model make unfair predictions on test nodes, where the victim model is trained with fairness consideration on the clean graph. Note that it is possible for real-world attackers to attack the access control of the databases to modify the input graph data, especially for edge computing systems with a coarse-grained access control (Ali et al., 2016; Xiao et al., 2019). In addition, once the model is deployed, the attacker can launch evasion attacks *at any time*, which increases the difficulty and cost of defending against evasion attacks (Zhang et al., 2022). Considering the severe impact of evasion attacks, many prevalent existing works Dai et al. (2018); Zügner et al. (2018); Zügner & Günnemann (2019); Zhang et al. (2022) make great efforts to study evasion attacks. In the fairness poisoning attack, the attacker's goal is to let the victim model make unfair predictions on test nodes, where the victim model is trained with fairness consideration on the poisoned graph. For both settings, we use commonly used fairness metrics, e.g., demographic parity (Dwork et al., 2012) and equal opportunity (Hardt et al., 2016) to measure the fairness of predictions.

Attacker's Knowledge. To make our attack practical in the real world, we set several limitations on the attacker's knowledge and formulate the attack within a gray-box setting. It is worth noting that our attacker's knowledge basically follows previous attacks on prediction utility of GNNs (Wu et al., 2019; Xu et al., 2019; Zügner & Günnemann, 2019; Chang et al., 2020a; Ma et al., 2020; Li et al., 2022a; Ma et al., 2022; Lin et al., 2022). Specifically, the attacker is able to observe the node attributes $\mathbf{X}$, graph structure $\mathbf{A}$, ground truth labels $\mathcal{Y}$, and sensitive attribute value set $\mathcal{S}$, but cannot observe the victim GNN model $f_{\boldsymbol{\theta}}$. Therefore, the attackers need to exploit a surrogate model $g_{\boldsymbol{\theta}}$ to achieve their goal.

It is worth noting that our method can be *directly* adapted to a white-box setting by replacing the trained surrogate model in the attacker's objective with the true victim model in Problem 1. In contrast, designing fairness attacks in a black-box attack setting can be extremely challenging. The difference between gray-box attacks and black-box attacks is black-box attackers are not allowed to access the ground truth labels. Different from node embeddings which can be obtained in an unsupervised way, group fairness metrics have to rely on the ground truth labels, which makes existing black-box attacks on graphs difficult to adapt to fairness attacks. Despite the difficulty of black-box fairness attacks, we provide an initial step toward a potential way to extend our framework to a black-box setting. First, the attacker can collect some data following a similar distribution, i.e., if the original graph is a Citeseer citation network, the attacker can collect data from Arxiv; if the original graph is a Facebook social network, the attacker can collect data from Twitter (X). During the data collection (preprocessing), the dimension of collected node features should be aligned with the original graph. Then, the attacker can train a state-of-the-art inductive GNN model on the collected graph data and obtain the predicted labels on the original graph. Finally, the attacker can use the predicted labels as a pseudo label to implement our G-FairAttack on the original graph.

Attacker's Capability. Between attacking the graph structure and the node attributes, we only consider the structure attack as the structure perturbation in the discrete domain is more challenging to solve and the structure attack can be easily adapted to obtain the attribute attack. Hence, we consider that attackers can only modify the graph structure $\mathbf{A}$, i.e., adding new edges or cutting existing edges, consistent with many previous attacks on prediction utility of GNNs (Dai et al., 2018; Xu et al., 2019; Zügner & Günnemann, 2019; Wang & Gong, 2019; Bojchevski & Günnemann, 2019; Chang et al., 2020a). In addition, the structure perturbation should be unnoticeable. Existing attacks of GNNs (Zügner et al., 2018; Zügner & Günnemann, 2019; Dai et al., 2018; Bojchevski & Günnemann, 2019) proposed the following unnoticeable constraints: Δ edges are changed at most; there are no singleton nodes, i.e., nodes without neighbors after the attack; the degree distributions before and after the attack should be the same with high confidence. We follow these works to ensure the unnoticeability of our attack. More importantly, we propose an extra unnoticeable constraint to ensure the difference of the utility losses before and after the attack is less than ϵ. This unnoticeable utility constraint makes attacks on fairness difficult to recognize.

After clarifying detailed attack settings, we use Figure 1 to illustrate a toy example of our proposed attack problem. In Figure 1, We use squares to denote the sensitive group 0 and triangles to denote the sensitive group 1. We use blue to label class-0 nodes and orange to label class-1 nodes. We compute the demographic parity and the equal opportunity metrics (larger value means less fair) to evaluate the fairness of the model prediction. By modifying two edges (from left to right), the attacker can let the fairness-aware GNN make unfair predictions while preserving the accuracy.

C Fast Computation

C.1 Fast Computation Sketch

The goal of fast computation is to solve the problem $(u^t, v^t) \leftarrow \arg\max_{(u,v)\in\mathcal{C}^t} \tilde{r}^t(u,v)$ efficiently. According to the definition of $\tilde{r}^t(u,v)$, the computation of $\tilde{r}^t(u,v)$ depends on two loss functions: the attacker's objective $\mathcal{L}_f$ and the utility loss $\mathcal{L}$. Between them, $\mathcal{L}_f$ can be formulated as

$$\mathcal{L}_f\left(g_{\boldsymbol{\theta}^*}, \mathbf{A}, \mathbf{X}, \mathcal{Y}, \mathcal{V}_{\text{test}}, \mathcal{S}\right) = \left|\sum_{i\in\mathcal{V}_{\text{test}}} k_i \mathbb{I}_{\geq 0}\left(g_{\boldsymbol{\theta}^*}\left(\mathbf{A},\mathbf{X}\right)_{[i]}\right)\right|, \tag{11}$$

where $k_i = 1/\left|\mathcal{V}_0\cap\mathcal{V}_{\text{test}}\right|$ if $i\in\mathcal{V}_0$ and $k_i = -1/\left|\mathcal{V}_1\cap\mathcal{V}_{\text{test}}\right|$ if $i\in\mathcal{V}_1$. $\mathbb{I}_{\geq 0}(\cdot)$ denotes an indicator function where $\mathbb{I}_{\geq 0}(x) = 1$ if $x\geq 0$ and $\mathbb{I}_{\geq 0}(x) = 0$ otherwise. The other $\mathcal{L}$ can be formulated as

$$\begin{aligned}\mathcal{L}(g_{\boldsymbol{\theta}^*}, \mathbf{A}, \mathbf{X}, \mathcal{Y}, \mathcal{V}_{\text{train}}) = -\frac{1}{|\mathcal{V}_{\text{train}}|}\sum_{i\in\mathcal{V}_{\text{train}}} & y_i \log\left(\sigma(g_{\boldsymbol{\theta}^*}(\mathbf{A},\mathbf{X})_{[i]})\right) \\ & + (1-y_i)\log\left(1-\sigma(g_{\boldsymbol{\theta}^*}(\mathbf{A},\mathbf{X})_{[i]})\right),\end{aligned} \tag{12}$$

Algorithm 1 G-FairAttack: A Sequential Attack on Fairness of GNNs.

```
Input: Clean adjacency matrix $\mathbf{A}$, attribute matrix $\mathbf{X}$, attack budget $\Delta$, utility budget $\epsilon$.
Output: The solution of Problem 1: $\mathbf{A}^*$.
1: $t \leftarrow 0, \mathcal{C}^0 \leftarrow \mathcal{E}, \mathbf{A}^0 \leftarrow \mathbf{A}$
2: $\boldsymbol{\theta}^0 \leftarrow \arg\min_{\boldsymbol{\theta}} \mathcal{L}_s(g_{\boldsymbol{\theta}}, \mathbf{A}, \mathbf{X}, \mathcal{Y}, \mathcal{S})$
3: while $t \le \Delta$ and $\left|\mathcal{L}(g_{\boldsymbol{\theta}^t}, \mathbf{A}^t) - \mathcal{L}(g_{\boldsymbol{\theta}^0}, \mathbf{A}^0)\right| \le \epsilon$ do
4:     $(u^t, v^t) \leftarrow \arg\max_{(u,v)\in\mathcal{C}^t} \tilde{r}^t(u,v)$, according to Algorithm 2.
5:     $\mathbf{A}^{t+1} \leftarrow flip_{(u^t,v^t)}\mathbf{A}^t$
6:     $\boldsymbol{\theta}^{t+1} \leftarrow \begin{cases} \boldsymbol{\theta}^t, & \textbf{Evasion} \\ \arg\min_{\boldsymbol{\theta}} \mathcal{L}_s\left(g_{\boldsymbol{\theta}}, \mathbf{A}^{t+1}, \mathbf{X}, \mathcal{Y}, \mathcal{S}\right), & \textbf{Poisoning} \end{cases}$
7:     $\mathcal{C}^{t+1} \leftarrow \mathcal{C}^t \backslash \{(u^t, v^t), (v^t, u^t)\}$
8:     $t \leftarrow t + 1$
9: end while
10: $\mathbf{A}^* \leftarrow \mathbf{A}^t$
```

where $\sigma(\cdot)$ denotes the sigmoid function. In the t-th iteration of our sequential attack, to compute the score function $\tilde{r}^t(u,v)$ efficiently, we should reduce the complexity of computing both $\Delta\mathcal{L}^t(u,v)$ and $\Delta\mathcal{L}^t_f(u,v)$. Specifically, our solution is to compute $flip_{(u,v)}\mathbf{Z}^t$ incrementally and obtain $g_{\boldsymbol{\theta}^t}(flip_{(u,v)}\mathbf{A}^t, \mathbf{X}) = flip_{(u,v)}\mathbf{Z}^t\boldsymbol{\theta}^t$. Then we can compute $\Delta\mathcal{L}_f(u,v)$ and $\Delta\mathcal{L}_(u,v)$ according to Equation (11) and Equation (12). We first review the computation of $flip_{(u,v)}\mathbf{Z}^t$ when *a new edge* (u,v) *is added.*

Case 1: If $i \in \{u, v\}$, we can compute $flip_{(u,v)}\mathbf{Z}^t_{[i,:]}$ as

$$flip_{(u,v)}\mathbf{Z}^t_{[i,:]} = \frac{\hat{\boldsymbol{d}}^t_{[i]}}{\hat{\boldsymbol{d}}^t_{[i]}+1}(\mathbf{Z}^t_{[i,:]} - \frac{\hat{\mathbf{A}}^t_{[i,:]}\mathbf{X}}{(\hat{\boldsymbol{d}}^t_{[i]})^2}) + \frac{\hat{\mathbf{A}}^t_{[i,:]}\mathbf{X}+\mathbf{X}_{[j,:]}}{(\hat{\boldsymbol{d}}^t_{[i]}+1)^2} + \frac{\hat{\mathbf{A}}^t_{[j,:]}\mathbf{X}+\mathbf{X}_{[i,:]}}{(\hat{\boldsymbol{d}}^t_{[i]}+1)(\hat{\boldsymbol{d}}^t_{[j]}+1)}, \tag{13}$$

where $j = v$ if $i = u$ and $j = u$ otherwise;

Case 2: If $i \in \mathcal{N}^t_u \cup \mathcal{N}^t_v \backslash \{u, v\}$, we can compute $flip_{(u,v)}\mathbf{Z}^t_{[i,:]}$ as

$$flip_{(u,v)}\mathbf{Z}^t_{[i,:]} = \mathbf{Z}^t_{[i,:]} - \mathbb{I}_{i\in\mathcal{N}^t_u}\cdot(\frac{\hat{\mathbf{A}}^t_{[u,:]}\mathbf{X}}{\hat{\boldsymbol{d}}^t_{[i]}\hat{\boldsymbol{d}}^t_{[u]}} - \frac{\hat{\mathbf{A}}^t_{[u,:]}\mathbf{X}+\mathbf{X}_{[v,:]}}{\hat{\boldsymbol{d}}^t_{[i]}(\hat{\boldsymbol{d}}^t_{[u]}+1)}) - \mathbb{I}_{i\in\mathcal{N}^t_v}\cdot(\frac{\hat{\mathbf{A}}^t_{[v,:]}\mathbf{X}}{\hat{\boldsymbol{d}}^t_{[i]}\hat{\boldsymbol{d}}^t_{[v]}} - \frac{\hat{\mathbf{A}}^t_{[v,:]}\mathbf{X}+\mathbf{X}_{[u,:]}}{\hat{\boldsymbol{d}}^t_{[i]}(\hat{\boldsymbol{d}}^t_{[v]}+1)}), \tag{14}$$

where $\mathbb{I}_{i\in\mathcal{N}} = 1$ if $i \in \mathcal{N}$, and $\mathbb{I}_{i\in\mathcal{N}} = 0$ otherwise;

Case 3: If $i \notin \mathcal{N}^t_u \cup \mathcal{N}^t_v$, we have $flip_{(u,v)}\mathbf{Z}^t_{[i,:]} = \mathbf{Z}^t_{[i,:]}$.

Next, we introduce the computation of $flip_{(u,v)}\mathbf{Z}^t$ when *an existing edge* (u,v) *is removed.* Similarly, we divide the computation into three cases as follows.

Case 1: If $i \in \{u, v\}$, we can compute $flip_{(u,v)}\mathbf{Z}^t_{[i,:]}$ as

$$flip_{(u,v)}\mathbf{Z}^t_{[i,:]} = \frac{\hat{\boldsymbol{d}}^t_{[i]}}{\hat{\boldsymbol{d}}^t_{[i]}-1}(\mathbf{Z}^t_{[i,:]} - \frac{\hat{\mathbf{A}}^t_{[i,:]}\mathbf{X}}{(\hat{\boldsymbol{d}}^t_{[i]})^2} - \frac{\hat{\mathbf{A}}^t_{[j,:]}\mathbf{X}}{\hat{\boldsymbol{d}}^t_{[i]}\hat{\boldsymbol{d}}^t_{[j]}}) + \frac{\hat{\mathbf{A}}^t_{[i,:]}\mathbf{X}-\mathbf{X}_{[j,:]}}{(\hat{\boldsymbol{d}}^t_{[i]}-1)^2}, \tag{15}$$

where $j = v$ if $i = u$ and $j = u$ otherwise;

Case 2: If $i \in \mathcal{N}^t_u \cup \mathcal{N}^t_v \backslash \{u, v\}$, we can compute $flip_{(u,v)}\mathbf{Z}^t_{[i,:]}$ as

$$flip_{(u,v)}\mathbf{Z}^t_{[i,:]} = \mathbf{Z}^t_{[i,:]} - \mathbb{I}_{i\in\mathcal{N}^t_u}\cdot(\frac{\hat{\mathbf{A}}^t_{[u,:]}\mathbf{X}}{\hat{\boldsymbol{d}}^t_{[i]}\hat{\boldsymbol{d}}^t_{[u]}} - \frac{\hat{\mathbf{A}}^t_{[u,:]}\mathbf{X}-\mathbf{X}_{[v,:]}}{\hat{\boldsymbol{d}}^t_{[i]}(\hat{\boldsymbol{d}}^t_{[u]}-1)}) - \mathbb{I}_{i\in\mathcal{N}^t_v}\cdot(\frac{\hat{\mathbf{A}}^t_{[v,:]}\mathbf{X}}{\hat{\boldsymbol{d}}^t_{[i]}\hat{\boldsymbol{d}}^t_{[v]}} - \frac{\hat{\mathbf{A}}^t_{[v,:]}\mathbf{X}-\mathbf{X}_{[u,:]}}{\hat{\boldsymbol{d}}^t_{[i]}(\hat{\boldsymbol{d}}^t_{[v]}-1)}), \tag{16}$$

where $\mathbb{I}_{i\in\mathcal{N}} = 1$ if $i \in \mathcal{N}$, and $\mathbb{I}_{i\in\mathcal{N}} = 0$ otherwise;

Case 3: If $i \notin \mathcal{N}^t_u \cup \mathcal{N}^t_v$, we have $flip_{(u,v)}\mathbf{Z}^t_{[i,:]} = \mathbf{Z}^t_{[i,:]}$.

The overall fast computation algorithm is shown in Algorithm 2, where argmax$_{@a}\rho^t(u,v)$ is denoted as the set of (u,v) corresponding to the top-a elements of $\rho^t(u,v)$.

Algorithm 2 The fast computation algorithm of (u^t, v^t).

```
Input: Adjacency matrix $\mathbf{A}^t$, attribute matrix $\mathbf{X}$, output matrix $\mathbf{Z}^t$, degree vector $\hat{\boldsymbol{d}}^t$, product matrix $\hat{\mathbf{A}}^t\mathbf{X}$, model parameter $\boldsymbol{\theta}^t$.
Output: Target edge $(u^t, v^t)$ in Algorithm 1.
1: $\mathcal{C}^t \leftarrow \underset{(u,v)\in\mathcal{E}^t}{\text{argmax}_{@a}} \rho^t(u,v)$.
2: $k \leftarrow 0$, $\boldsymbol{p}^t \leftarrow \mathbf{0}$, $\boldsymbol{q}^t \leftarrow \mathbf{0}$.
3: for $(u,v) \in \mathbf{C}^t$ do
4:     $flip_{(u,v)}\mathbf{Z}^t \leftarrow \mathbf{Z}^t$
5:     for $i \in \mathcal{N}_u^t \cup \mathcal{N}_v^t$ do
6:         if $i \in \{u,v\}$ then
7:             Update $flip_{(u,v)}\mathbf{Z}^t_{[i,:]}$ according to Equation (13) or Equation (15).
8:         else
9:             Update $flip_{(u,v)}\mathbf{Z}^t_{[i,:]}$ according to Equation (14) or Equation (16).
10:        end if
11:    end for
12:    $g_{\boldsymbol{\theta}^t}(flip_{(u,v)}\mathbf{A}^t, \mathbf{X}) \leftarrow flip_{(u,v)}\mathbf{Z}^t\boldsymbol{\theta}^t$
13:    Compute $\mathcal{L}(flip_{(u,v)}\mathbf{A}^t, \mathbf{X})$ and $\mathcal{L}_f(flip_{(u,v)}\mathbf{A}^t, \mathbf{X})$ according to Equation (11) and Equation (12).
14:    $\boldsymbol{p}^t_{[k]} \leftarrow \mathcal{L}(flip_{(u,v)}\mathbf{A}^t, \mathbf{X}) - \mathcal{L}(\mathbf{A}^t, \mathbf{X})$
15:    $\boldsymbol{q}^t_{[k]} \leftarrow \mathcal{L}_f(flip_{(u,v)}\mathbf{A}^t, \mathbf{X}) - \mathcal{L}_f(\mathbf{A}^t, \mathbf{X})$
16:    $k \leftarrow k+1$
17: end for
18: $\tilde{\boldsymbol{r}}^t \leftarrow \boldsymbol{q}^t - \frac{(\boldsymbol{p}^t)^T\boldsymbol{q}^t}{\|\boldsymbol{p}^t\|_2^2}\boldsymbol{p}^t$
19: $i_{\text{max}} \leftarrow \arg\max_{i=0,\ldots,|\mathcal{C}^t|-1} \tilde{\boldsymbol{r}}^t_{[i]}$
20: $(u^t, v^t) \leftarrow \mathcal{C}^t_{[i_{\text{max}}]}$
```

C.2 Complexity Analysis

Based on Algorithm 2, we provide a detailed complexity analysis for our proposed G-FairAttack.

Proposition 2. *The overall time complexity of G-FairAttack with the fast computation is $O(\bar{d}n^2 + d_x an)$, where $\bar{d}$ denotes the average degree.*

Proof. First, to compute $\mathcal{C}^t$, we compute $|\mathbf{Z}^t\boldsymbol{\theta}^t|$ and find the maximum M_t in $O(d_x n)$. Then we compute $\rho^t(u,v) = \sum_{i\in\mathcal{N}_u^t\cup\mathcal{N}_v^t} M_t - |\mathbf{Z}^t_{[i,:]}\boldsymbol{\theta}^t|$ for $(u,v) \in \mathcal{E}^t$ in $O(\bar{d}n^2)$, and find the top-a elements as $\mathcal{C}^t$ in $O(n\log a)$. Then, the computation of $\boldsymbol{p}^t$ and $\boldsymbol{q}^t$ can be divided into the following steps for each edge $(u,v) \in \mathcal{C}^t$.

1. The computation of $flip_{(u,v)}\mathbf{Z}^t_{[i,:]}$ for $i \in \mathcal{N}_u^t \cup \mathcal{N}_v^t$. We can store and update $\hat{\mathbf{A}}^t\mathbf{X}$, $\hat{\boldsymbol{d}}^t$, and $\mathbf{Z}^t$ for each iteration. Hence, the computation of Equation (13), Equation (14), Equation (15), and Equation (16) only requires $O(1)$. Consequently, the total time complexity of this step is $O(\bar{d})$.
2. The computation of $g_{\boldsymbol{\theta}^t}(flip_{(u,v)}\mathbf{A}^t, \mathbf{X}) = flip_{(u,v)}\mathbf{Z}^t\boldsymbol{\theta}^t$ requires $O(nd_x)$.
3. According to Equation (11) and Equation (12), the computation of the loss functions $\mathcal{L}(flip_{(u,v)}\mathbf{A}^t, \mathbf{X})$ and $\mathcal{L}_f(flip_{(u,v)}\mathbf{A}^t, \mathbf{X})$ based on $g_{\boldsymbol{\theta}^t}(flip_{(u,v)}\mathbf{A}^t, \mathbf{X})$ requires $O(n)$.

Considering all edges from $\mathcal{C}^t$, the computation of $\boldsymbol{p}^t$ and $\boldsymbol{q}^t$ requires $O(d_x an)$. Finally, we can compute $\tilde{\boldsymbol{r}}^t$ and find (u^t, v^t) in $O(a)$. Combining all these steps, the complexity of Algorithm 2 is $O(\bar{d}n^2 + d_x an)$ in total. □

With our fast computation method, the total time complexity of G-FairAttack is $O((\bar{d}n^2 + d_x an)\Delta)$. Here, the retraining of the surrogate model $\boldsymbol{\theta}^{t+1} = \arg\min_{\boldsymbol{\theta}} \mathcal{L}_s\left(g_{\boldsymbol{\theta}}, \mathbf{A}^{t+1}, \mathbf{X}, \mathcal{Y}, \mathcal{S}\right)$ in the fairness poisoning attack is neglected because the convergence is not controllable. The overall G-FairAttack algorithm is shown in Algorithm 1. We can obtain the space complexity of G-FairAttack as $O(|\mathcal{E}| + d_x n)$.

Next, we show that our complexity can be further reduced in practice. We list two potential ways as follows.

1. The first approach is to implement our fast computation algorithm in parallel. As the proof of Proposition 2 shows, the main part of G-FairAttack's complexity is the computation of $\rho^t(u, v)$ for $(u, v) \in \mathcal{E}^t$, which has $O(\bar{d}n^2)$ complexity. It is distinct that this computation can be implemented in parallel where $\mathcal{E}^t$ is partitioned into p subsets, and each subset is fed into one process. By exploiting parallel computation, the overall complexity can be reduced to $O(\bar{d}n^2/p)$.
2. Instead of ranking all of the edges in $\mathcal{E}^t$ by $\rho^t(u, v)$, we can just randomly sample a edges from $\mathcal{E}^t$ as C^t. By using random sampling instead of ranking, the overall complexity can be reduced to $O(d_x a n)$. However, the error of the fast computation might increase without a careful choice of the sampling distribution.

Note that most existing adversarial attack approaches (Zügner et al., 2018; Zügner & Günnemann, 2019; Bojchevski & Günnemann, 2019; Lin et al., 2022) do not have a lower complexity (less than $O(n^2)$) than our proposed G-FairAttack. The adversarial attacks with an $O(n^2)$ complexity can already fit most commonly used graph datasets. In general, our method is practical for most graph datasets as the existing literature. For extremely large datasets, we can also use the aforementioned strategies to reduce further the time complexity.

Finally, we would like to make a more detailed comparison of the time complexity with adopted attacking baselines. The random sampling-based baselines, i.e., random and FA-GNN, definitely have lower time complexity ($O(\Delta)$, Δ is the attack budget) because they are based on random sampling. Although their complexity is low, the effectiveness of random sampling-based attacks is very limited. For the rest gradient-based attack baselines, i.e., Gradient Ascent and Metattack, their time complexities are $O(n^2)$ (Zügner & Günnemann, 2019), the same as G-FairAttack. However, gradient-based methods have a larger space complexity compared with G-FairAttack ($O(n^2)$ vs. $O(d_x n + |\mathcal{E}|)$).

D G-FairAttack vs Gradient-based Methods

The fairness attack of GNNs is a discrete optimization problem, which is highly challenging to solve. Most of the existing adversarial attacks that focus on the prediction utility of GNNs adopt gradient-based methods (Zügner & Günnemann, 2019; Wu et al., 2019; Xu et al., 2019; Geisler et al., 2021) to find the maximum of the attacker's objective. As G-FairAttack, gradient-based structure attacks flip the edges sequentially. In the t-th iteration ($t = 1, 2, \dots$), the gradient-based optimization algorithm finds a target edge (u^t, v^t) based on the gradient of the adjacency matrix $\nabla_{\mathbf{A}^t}\mathcal{L}$ where $\mathcal{L}$ is the objective function of the attacker, and flips this target edge to obtain the update adjacency matrix $\mathbf{A}^{t+1}$, which is expected to increase the attacker's objective. In particular, to obtain $\nabla_{\mathbf{A}^t}\mathcal{L}$, gradient-based methods extend the discrete adjacency matrix $\mathbf{A}^t \in \{0, 1\}^{n\times n}$ to a continuous domain $\mathbb{R}^{n\times n}$ and compute $\nabla_{\mathbf{A}^t}\mathcal{L} \in \mathbb{R}^{n\times n}$. Specifically, for poisoning attacks where the problem becomes a bilevel optimization, existing methods exploit the meta-learning (Zügner & Günnemann, 2019) or the convex relaxation (Xu et al., 2019) techniques to remove the inner optimization. After obtaining $\nabla_{\mathbf{A}^t}\mathcal{L}$, the gradient-based methods should update $\mathbf{A}^t$ in the discrete domain instead of using gradient ascent directly. Specifically, gradient-based methods choose the target edge *corresponding to the largest element* or use random sampling to find a target element $\mathbf{A}^t_{[u,v]}$.

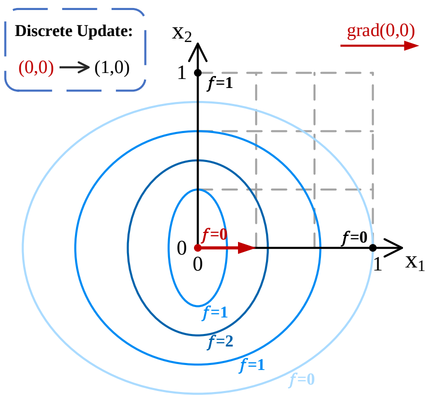

Figure 4: The limitation of the gradient-based optimization method. The blue ellipses are isolines of the loss function.

Although existing attacks of GNNs based on gradient-based methods successfully decrease the prediction utility of victim models, they have two main limitations.

The first limitation is that we cannot ensure the loss function after flipping the target edge will increase because the update in the discrete domain brings an uncontrollable error. The intuition of the gradient-based method is that we cannot update the adjacency matrix with gradient ascent because the adjacency matrix is binary and only one edge can be flipped in each time. Hence, we expect that flipping the target edge corresponding to the largest gradient component can lead to the largest increment of the attacker's objective $\mathcal{L}(\mathbf{A}, \mathbf{X})$. However, this expectation can be false since the update of the adjacency matrix (flipping one target edge) has a fixed length. Next, we prove Proposition 1.

Proposition 1. *Gradient-based methods for optimizing the graph structure are not guaranteed to decrease the objective function.*

Proof. Consider the loss function $\mathcal{L}(\mathbf{A}, \mathbf{X})$ near a specific point $\mathbf{A}_0$ where $\mathbf{A} \in \mathbb{R}^{n^2}$ is a vectorized adjacency matrix. Based on Taylor's Theorem, we have

$$\mathcal{L}(\mathbf{A}, \mathbf{X}) = \mathcal{L}(\mathbf{A}_0, \mathbf{X}) + \nabla_{\mathbf{A}}\mathcal{L}(\mathbf{A}_0, \mathbf{X})^\top(\mathbf{A} - \mathbf{A}_0) + R_1(\mathbf{A}),$$

where $R_1(\mathbf{A}) = h_1(\mathbf{A})\|\mathbf{A} - \mathbf{A}_0\|$ is the Peano remainder and we have $\lim_{\mathbf{A}\to\mathbf{A}_0} h_1(\mathbf{A}) = 0$. For gradient-based methods, we have $\mathbf{A}_1 = \mathbf{A}_0 + \boldsymbol{e}_k$ where $\boldsymbol{e}_k$ is the basis vector at the k-th dimension. Then, we have

$$\mathcal{L}(\mathbf{A}_1, \mathbf{X}) = \mathcal{L}(\mathbf{A}_0, \mathbf{X}) + \nabla_{\mathbf{A}}\mathcal{L}(\mathbf{A}_0, \mathbf{X})[k] + h_1(\mathbf{A}_1).$$

Here, we know that $\nabla_{\mathbf{A}}\mathcal{L}(\mathbf{A}_0, \mathbf{X})[k]$ is the largest positive element of $\nabla_{\mathbf{A}}\mathcal{L}(\mathbf{A}_0, \mathbf{X})$, which is a fixed value. Then, we expect that choosing $\mathbf{A}_1$ can lead to the fact that $\mathcal{L}(\mathbf{A}_1, \mathbf{X}) > \mathcal{L}(\mathbf{A}_0, \mathbf{X})$, i.e., $\nabla_{\mathbf{A}}\mathcal{L}(\mathbf{A}_0, \mathbf{X})[k] + h_1(\mathbf{A}_1) > 0$. However, this inequality is not true without further assumptions when $\|\mathbf{A}_1 - \mathbf{A}_0\|_0 = 1$. □

In comparison, we also show that the error can be controlled in the continuous domain by a careful selection of the learning rate. In the continuous domain, the situation is different because we can make the value of $\|\mathbf{A}_1 - \mathbf{A}_0\|$ arbitrarily small by tuning the learning rate η where $\mathbf{A}_1 = \mathbf{A}_0 + \eta\nabla_{\mathbf{A}}\mathcal{L}(\mathbf{A}_0, \mathbf{X})[k]\boldsymbol{e}_k$. Note that we have $\lim_{\mathbf{A}\to\mathbf{A}_0} h_1(\mathbf{A}) = 0$ and the value of $\nabla_{\mathbf{A}}\mathcal{L}(\mathbf{A}_0, \mathbf{X})[k]$ is fixed. Hence we can choose a proper η which makes $\|\mathbf{A}_1 - \mathbf{A}_0\|$ small enough to ensure $|h_1(\mathbf{A}_1)| < \nabla_{\mathbf{A}}\mathcal{L}(\mathbf{A}_0, \mathbf{X})[k]$. Finally, we have $\nabla_{\mathbf{A}}\mathcal{L}(\mathbf{A}_0, \mathbf{X})[k] + h_1(\mathbf{A}_1) > 0$ and $\mathcal{L}(\mathbf{A}_1, \mathbf{X}) > \mathcal{L}(\mathbf{A}_0, \mathbf{X})$ consequently. We also provide a two-dimensional case in Figure 4. In the iteration, the optimization starts at $(0, 0)$. The gradient at $(0, 0)$ is $[1\ 0]^\top$. According to the gradient-based methods, the next point should be at $(1, 0)$. However, the loss after updating does not increase $f(1, 0) = f(0, 0)$. Instead, $(0, 1)$ is a better update for $f(0, 1) > f(0, 0)$ in this iteration.

The second limitation is the large space complexity. The computation of $\nabla_{\mathbf{A}^t}\mathcal{L}$ requires storing a dense adjacency matrix with $O(n^2)$ space complexity, which is costly at a large scale.

In contrast, our proposed G-FairAttack successfully addresses these limitations. First, G-FairAttack can ensure the increase of the attacker's objective after flipping the target edge since G-FairAttack exploits a ranking-based method to choose the target edge in each iteration. In particular, we choose the target edge as $\max_{(u,v)\in\mathcal{C}^t} r^t(u, v) = \mathcal{L}_f(g_{\boldsymbol{\theta}^t}, flip_{(u,v)}\mathbf{A}^t) - \mathcal{L}_f(g_{\boldsymbol{\theta}^t}, \mathbf{A}^t)$, which ensures that flipping the target edge can maximize the increment of attacker's objective. Second, unlike gradient-based methods, G-FairAttack does not require storing a dense adjacency matrix as no gradient computations are involved. Referring to the discussion in Appendix C.2, the space complexity of G-FairAttack is $O(|\mathcal{E}| + d_x n)$, much lower than gradient-based methods ($O(n^2)$). Moreover, we conduct an experiment to demonstrate the superiority of G-FairAttack compared with gradient-based optimization methods. Specifically, we compare the effectiveness of G-FairAttack with two gradient-based optimization methods in both fairness evasion attack and fairness poisoning attack settings. If an optimization algorithm leads to a larger increase in the attacker's objective, it is more effective. For the fairness evasion attack, we choose Gradient Ascent as the baseline method. Given the attack budget $\Delta = 0.5\%|\mathcal{E}|$, we record the value of the attacker objective $\mathcal{L}_f(g_{\boldsymbol{\theta}^*}, \mathbf{A}^t)$, i.e., demographic parity based on a surrogate model in the t-th iteration, for $t = 0, \ldots, \Delta$. The result is shown in Figure 5(a). We observe that the attacker objective keeps increasing during our non-gradient optimization (adopted by G-FairAttack) process and reaches an optimum rapidly, while the gradient-based optimization method (adopted by Gradient Ascent) cannot ensure the increment of the attacker objective during the optimization.

Table 3: Dataset statistics.

Dataset	#Nodes	#Edges	#Attributes	#Train/%	#Validation/%	#Test/%	Sensitive
Facebook	1,045	53,498	574	50%	20%	30%	Gender
Pokec	7,659	41,100	277	13%	25%	25%	Region
Credit	30,000	200,526	13	20%	20%	30%	Age

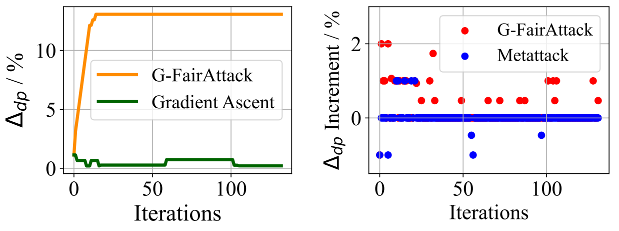

(a) Fairness evasion attack. (b) Fairness poisoning attack.

Figure 5: The variation of attacker's objective during the optimization process on Facebook, comparing non-gradient methods (G-FairAttack) with gradient-based methods (Gradient Ascent, Metattack).

For the fairness poisoning attack, we choose Metattack as the baseline method. During the optimization process, the surrogate model $g_{\boldsymbol{\theta}_t}$ is retrained in each iteration. The convergence of the surrogate model during the retraining is not controllable. To make a fair comparison, we should ensure both optimization methods compute the attacker objective based on the same surrogate model. Hence we fix $\mathbf{A}^t$ and $g_{\boldsymbol{\theta}^t}$ for both methods and record the increment of the attacker objective $\mathcal{L}_f(g_{\boldsymbol{\theta}^t}, \mathbf{A}^{t+1}) - \mathcal{L}_f(g_{\boldsymbol{\theta}^t}, \mathbf{A}^t)$ in the t-th iteration, for $t = 0, \dots, \Delta$, where $\mathbf{A}^{t+1}$ is obtained based on different optimization methods. In conclusion, we compare the increment of the attacker's objective caused by a single optimization step of different optimization methods in this case. The result is shown in Figure 5(b). For G-FairAttack, the attacker's objective increases in 28 iterations, i.e., positive Δ_{dp} variation, and decreases in 1 iteration. For Metattack, the attacker objective increases in only 5 iterations and decreases in 5 iterations as well. Therefore, a single step of G-FairAttack leads to a larger increase of the attacker's objective than Metattack given the same initial point $\mathbf{A}^t$. In conclusion, our proposed G-FairAttack leads to a better solution in the optimization process compared with gradient-based methods in both fairness evasion attacks and fairness poisoning attacks.

E Implementation Details

E.1 Datasets

The statistics of these datasets are shown in Table 3. In the Facebook graph (Leskovec & Mcauley, 2012), the nodes represent user accounts of Facebook, and the edges represent the friendship relations between users. Node attributes are collected from user profiles. The sensitive attributes of user nodes are their genders. The task of Facebook is to predict the education type of the users. In the Credit defaulter graph (Dai & Wang, 2021), the nodes represent credit card users, and the edges represent whether two users are similar or not according to their spending and payment patterns. The sensitive attributes of user nodes are their ages. The task of Credit is to predict whether a user will default on the credit card payment or not. In the Pokec graph (Agarwal et al., 2021), the nodes represent user accounts of a prevalent social network in Slovakia, and the edges represent the friendship relations between users. The sensitive attributes of user nodes are their regions. The task of Pokec is to predict the working fields of the users. It is worth noting that we use a subgraph of Pokec in (Dong et al., 2022a) instead of the original version in (Dai & Wang, 2021). In our experiment implementation, we adopt the *PyGDebias* library (Dong et al., 2023a) to load these datasets.

E.2 Baselines

We first introduce the detailed settings of the attack baselines in the first stage of evaluation.

- Random (Zügner et al., 2018; Hussain et al., 2022): Given the attack budget Δ, we randomly flip Δ edges (removing existing edges or adding new edges) and obtain the attacked graph. It is a random method that fits both the fairness evasion attack setting and the fairness poisoning attack setting.

- FA-GNN (Hussain et al., 2022): Given the attack budget Δ, we randomly link Δ pairs of nodes that belong to different classes and different sensitive groups. Specifically, we choose the most effective link strategy, "DD", in our experiments. It is also a random method that fits both attack settings.
- Gradient Ascent: Given the attack budget Δ, we flip Δ edges sequentially in Δ iterations. In each iteration, we compute the gradient $\nabla_{\mathbf{A}'}\mathcal{L}_f(g_{\boldsymbol{\theta}^*}, \mathbf{A}')$ and flip one edge corresponding to the largest element of the gradient, where $\boldsymbol{\theta}^* = \arg\min_{\boldsymbol{\theta}} \mathcal{L}_s(g_{\boldsymbol{\theta}}, \mathbf{A})$. To make $\mathcal{L}_f$ differentiable, we use the soft predictions to substitute the prediction labels in $\mathcal{L}_f$ as (Zeng et al., 2021). Here, we choose a two-layer graph convolutional network (Kipf & Welling, 2017) as the surrogate model $g_{\boldsymbol{\theta}}$, and CE loss as the surrogate loss function $\mathcal{L}_s$. Gradient Ascent is an optimization-based method that only fits the fairness evasion attack setting.
- Metattack (Zügner & Günnemann, 2019): Given the attack budget Δ, we sequentially flip Δ edges in Δ iterations. In each iteration, we compute the meta gradient $\nabla_{\mathbf{A}'}\mathcal{L}_f(g_{\boldsymbol{\theta}^*}(\mathbf{A}'), \mathbf{A}')$ by MAML (Finn et al., 2017) and flip one edge corresponding to the largest element of the meta gradient, where $\boldsymbol{\theta}^* = \arg\min_{\boldsymbol{\theta}} \mathcal{L}_s(g_{\boldsymbol{\theta}}, \mathbf{A}')$. To make $\mathcal{L}_f$ differentiable, we implement the same adaption of $\mathcal{L}_f$ as Gradient Ascent. Here, we also choose a two-layer GCN as the surrogate model $g_{\boldsymbol{\theta}}$ and CE loss as the surrogate loss function $\mathcal{L}_s$. Metattack is also an optimization-based method, while it only fits the fairness poisoning attack.

It is worth noting that for both Gradient Ascent and Metattack, we should flip the sign of the gradient components for connected node pairs as this yields the gradient for a change in the negative direction (i.e., removing the edge) (Zügner & Günnemann, 2019). Hence, we flip the edge corresponding to the largest score $\nabla_{\mathbf{A}_{[u,v]}}\mathcal{L}_f \cdot (-2 \cdot \mathbf{A}_{[u,v]} + 1)$ for $(u, v) \in \mathcal{E}$ for Gradient Ascent and Metattack.

Next, we introduce our adopted test GNNs in the second stage. We choose four types of GNNs, including a vanilla GNN and three types of fairness-aware GNNs.

- Vanilla: We choose a two-layer GCN (Kipf & Welling, 2017), which is a mostly adopted GNN model in existing works.
- Δ_{dp}: We choose the output-based regularization method (Navarin et al., 2020; Zeng et al., 2021; Wang et al., 2022a; Dong et al., 2023c). Specifically, we choose a two-layer GCN as the backbone and add a regularization term Δ_{dp} to the loss function. Moreover, to make the regularization term differentiable, we use the soft prediction to substitute the prediction label in Δ_{dp} as (Zeng et al., 2021).
- $I(\hat{Y}, S)$: For mutual information loss, except for directly decreasing the mutual information, the adversarial training (Bose & Hamilton, 2019; Dai & Wang, 2021) could also be seen as a specific case of exploiting the mutual information loss according to (Kang et al., 2022). In an adversarial training framework, an adversary is trained to predict S based on $\hat{Y}$. If the prediction is more accurate, it demonstrates that the output $\hat{Y}$ of the GNN contains more information about the sensitive attribute S, i.e., the GNN model is less fair. We choose FairGNN (Dai & Wang, 2021) as the baseline in the mutual information type. FairGNN contains a discriminator to predict the sensitive attribute based on the output of a GNN backbone. The GNN backbone is trained to fool the discriminator for predicting the sensitive attribute. Specifically, we choose a single-layer GCN as the GNN backbone.
- $W(\hat{Y}, S)$: We choose EDITS (Dong et al., 2022a), a model agnostic debiasing framework for GNNs. EDITS finds a debiased adjacency matrix and a debiased node attribute matrix by minimizing the Wasserstein distance of the distributions of node embeddings on different sensitive groups. With the debiased input graph data, the fairness of the GNN backbone is improved. Specifically, we choose a two-layer GCN as the GNN backbone.

E.3 Experimental Settings

The implementation of our experiments could be divided into two parts, fairness attack methods, and the test GNN models. For attack methods, we use the source code of FA-GNN (Hussain et al., 2022) and Metattack (Zügner & Günnemann, 2019). Other attack methods including G-FairAttack are implemented in PyTorch (Paszke et al., 2019). For test GNN models, we use the source code of GCN (Kipf & Welling, 2017), FairGNN (Dai & Wang, 2021), and EDITS (Dong et al., 2022a).

Table 4: The hyperparameter settings of four different types of test GNNs on three benchmarks in fairness evasion attack and fairness poisoning attack settings. The detailed definition and description of parameters α, β, μ_1, μ_2, μ_3, μ_4, and r refers to (Dai & Wang, 2021; Dong et al., 2022a).

Test GNN	Hyperparameter	Fairness Evasion Attack			Fairness Poisoning Attack		
		Facebook	Pokec	Credit	Facebook	Pokec	Credit
GCN	learning rate	$1e^{-4}$	$1e^{-4}$	$1e^{-2}$	$1e^{-4}$	$1e^{-3}$	$1e^{-3}$
	weight decay	$1e^{-5}$	$1e^{-2}$	$1e^{-5}$	$1e^{-5}$	$1e^{-5}$	$1e^{-5}$
	dropout	0.5	0.2	0.5	0.5	0.5	0.5
	epochs	2,000	1,000	1,000	1,000	500	200
Reg	learning rate	$1e^{-4}$	$1e^{-3}$	$5e^{-2}$	$1e^{-4}$	$1e^{-3}$	$5e^{-3}$
	weight decay	$1e^{-5}$	$1e^{-5}$	$1e^{-5}$	$1e^{-5}$	$1e^{-5}$	$1e^{-5}$
	dropout	0.5	0.2	0.2	0.5	0.5	0.5
	epochs	2,000	10,000	2,000	1,000	1,000	500
	fairness loss weight α	1	150	1	1	80	1
FairGNN	learning rate	$1e^{-3}$	$5e^{-3}$	$1e^{-2}$	$1e^{-4}$	$5e^{-3}$	$1e^{-3}$
	weight decay	$1e^{-5}$	$1e^{-5}$	$1e^{-5}$	$1e^{-5}$	$1e^{-5}$	$1e^{-5}$
	dropout	0.5	0.5	0.2	0.5	0.5	0.5
	epochs	2,000	5,000	1,000	1,500	5,000	1,000
	covariance constraint weight α	60	1	20	2	100	30
	adversarial debiasing weight β	10	500	10	3	1,000	1
EDITS	learning rate	$1e^{-4}$	$1e^{-4}$	$5e^{-3}$	$1e^{-3}$	$1e^{-4}$	$1e^{-3}$
	weight decay	$1e^{-5}$	$1e^{-5}$	$1e^{-5}$	$1e^{-5}$	$1e^{-5}$	$1e^{-5}$
	dropout	$5e^{-2}$	$5e^{-2}$	$5e^{-2}$	$5e^{-2}$	$5e^{-2}$	$5e^{-2}$
	epochs	1,000	500	500	2,000	1,000	200
	μ_1	$1e^{-2}$	$3e^{-2}$	$5e^{-2}$	$1e^{-2}$	$3e^{-2}$	$5e^{-2}$
	μ_2	0.8	70	0.1	0.8	70	0.1
	μ_3	0.1	1	1	0.1	1	1
	μ_4	20	15	15	20	15	15
	edge binarization threshold r	$1e^{-4}$	0.3	$5e^{-3}$	$1e^{-4}$	0.2	$2e^{-2}$

We exploit Adam optimizer (Kingma & Ba, 2015) to optimize the surrogate model, gradient-based attacks, and the test GNNs. All experiments are implemented on an Nvidia RTX A6000 GPU. We provide the hyperparameter settings of G-FairAttack in Table 5, and the hyperparameter settings of test GNNs in Table 4. [3]

E.4 Required Packages

We list some key packages in Python required for implementing G-FairAttack as follows.

- Python == 3.9.13
- torch == 1.11.0
- torch-geometric == 2.0.4
- numpy == 1.21.5
- numba == 0.56.3
- networkx == 2.8.4
- scikit-learn == 1.1.1
- scipy == 1.9.1
- dgl == 0.9.1
- deeprobust == 0.2.5

[3]The open-source code is available at https://github.com/zhangbinchi/G-FairAttack.

F Supplementary Experiments

F.1 Effectiveness of Attack

In Section 4.2, we discussed the effectiveness of G-FairAttack in attacking the fairness of different types of GNNs. Here, we provide more results of the same experiment as Section 4.2 but in different attack settings and more fairness metrics. Table 6 shows the experimental results of fairness evasion attacks in Δ_{eo} fairness metric, Table 7 shows the experimental results of fairness poisoning attacks in Δ_{dp} fairness metric, and Table 8 shows the experimental results of fairness poisoning attacks in Δ_{eo} fairness metric. From the results, we can find that the overall performance of G-FairAttack is better than any other baselines, which highlights the clear superiority of G-FairAttack. In addition, we can find that G-FairAttack seems less desirable in the cases where vanilla GCN serves as the victim model. The reason for this phenomenon is our surrogate loss contains two parts, utility loss term L and fairness loss term L_f, while the real victim loss of vanilla GCN only contains the utility loss term L. However, in the general case (without knowing the type of the victim model), G-FairAttack can outperform all other baselines when the surrogate loss differs from the victim loss (when attacking fairness-aware GNNs). Despite that, the shortage in attacking vanilla GNNs can be solved easily by choosing a smaller hyperparameter α (the weight of L_f). As Table 5 shows, we fix the hyperparameter setting (also fix α) for all attack methods when attacking different types of victim models because the attacker cannot choose different hyperparameters based on the specific type of the victim model in the gray-box attack setting. By fixing the hyperparameter settings for different victim models, the experimental results demonstrate that our G-FairAttack is **victim model-agnostic** and **easy to use** (in terms of hyperparameter tuning). In addition, we can also find that the fairness poisoning attack is a more challenging task (easier to fail), while effective fairness poisoning attack methods induce a more serious deterioration in the fairness of the victim model. Furthermore, we obtain that edge rewiring based methods (EDITS) can effectively defend against some fairness attacks (more details about this conclusion are discussed in Appendix G).

Table 5: The hyperparameter settings of G-FairAttack on three benchmarks. The "(s)" denotes that the corresponding hyperparameter is related to the training of the surrogate model.

Hyperparameter	Facebook	Pokec	Credit
attack budget Δ	5%	5%	1%
utility budget ϵ	5%	5%	5%
threshold a	0.1	$5e^{-3}$	$1e^{-4}$
learning rate (s)	$1e^{-3}$	$1e^{-3}$	$5e^{-2}$
weight decay (s)	$1e^{-5}$	$1e^{-5}$	$1e^{-5}$
epochs (s)	2,000	2,000	1,000
dropout (s)	0.5	0.5	0.5
fairness loss weight α (s)	1	1	1
bandwidth h (s)	0.1	0.1	0.1
number of intervals m (s)	10,000	10,000	1,000

F.2 Effectiveness of Surrogate Loss

In Section 4.3, we discussed the effectiveness of our proposed surrogate loss in representing different types of fairness loss in different victim models. Here, we provide more results of the same experiment as Section 4.3 but in different attack settings and datasets. Table 9 shows the experimental results of fairness evasion attacks on the Facebook dataset. As mentioned in Section 4.3, the surrogate loss function in the attack method and the victim loss function in the victim model are different in our attack setting. The attacker does not know the form of the victim loss function due to the gray-box setting. If the surrogate loss is the same as the victim loss, the attack method naturally can have a desirable performance (as white-box attacks). However, in this experiment, we demonstrate that G-FairAttack (with our proposed surrogate loss) has the most desirable performance when attacking different victim models **with a different victim loss** from the surrogate loss. Consequently, our experiment verifies that our surrogate loss function is adaptable to attacking different types of victim models.

Table 9: Results of G-FairAttack on Facebook while replacing the total variation loss with other loss terms.

Attack	FairGNN		EDITS	
	Δ_{dp} (%)	Δ_{eo} (%)	Δ_{dp} (%)	Δ_{eo} (%)
Clean	6.23 ± 0.69	4.78 ± 0.98	1.15 ± 0.25	2.31 ± 0.58
G-FA-None	6.35 ± 0.83	4.78 ± 0.98	4.19 ± 0.29	2.88 ± 0.33
G-FA-Δ_{dp}	6.35 ± 0.83	4.78 ± 0.98	3.86 ± 0.29	2.88 ± 0.33
G-FA	8.62 ± 0.91	5.70 ± 0.64	4.19 ± 0.29	2.88 ± 0.33

Table 6: Experiment results of fairness evasion attack, where AUC and Δ_{eo} are adopted as the prediction utility metric and the fairness metric, correspondingly.

Victim	Attack	Facebook		Pokec_z		Credit	
		AUC(%)	Δ_{eo}(%)	AUC(%)	Δ_{eo}(%)	AUC(%)	Δ_{eo}(%)
GCN	Clean	64.53 ± 0.05	0.52 ± 0.41	72.87 ± 0.20	8.75 ± 0.94	70.48 ± 0.14	12.29 ± 2.14
	Random	65.05 ± 0.10	1.55 ± 0.00	72.56 ± 0.20	**8.71 ± 2.50**	70.53 ± 0.13	12.57 ± 2.29
	FA-GNN	63.00 ± 0.06	2.12 ± 0.58	72.12 ± 0.28	1.31 ± 1.05	70.44 ± 0.12	**14.39 ± 2.65**
	Gradient Ascent	64.77 ± 0.11	1.93 ± 0.33	72.88 ± 0.18	5.93 ± 1.74	-	-
	G-FairAttack	64.20 ± 0.03	**2.38 ± 0.68**	72.91 ± 0.20	6.69 ± 1.63	70.44 ± 0.11	12.75 ± 2.12
Reg	Clean	64.09 ± 0.16	0.38 ± 0.00	71.08 ± 0.35	1.73 ± 1.15	70.26 ± 0.34	0.66 ± 0.84
	Random	64.49 ± 0.26	0.77 ± 0.33	70.86 ± 0.30	1.34 ± 1.12	70.31 ± 0.34	0.82 ± 0.98
	FA-GNN	62.28 ± 0.23	0.90 ± 0.78	70.12 ± 0.25	5.23 ± 0.38	70.34 ± 0.36	0.32 ± 0.27
	Gradient Ascent	64.40 ± 0.12	0.20 ± 0.00	71.21 ± 0.49	2.25 ± 1.19	-	-
	G-FairAttack	63.30 ± 0.14	**1.74 ± 0.33**	71.11 ± 0.26	**7.14 ± 1.26**	70.21 ± 0.37	**2.08 ± 1.20**
FairGNN	Clean	65.24 ± 0.49	0.97 ± 0.77	69.71 ± 0.09	0.81 ± 0.69	67.32 ± 0.46	0.94 ± 0.67
	Random	64.88 ± 0.52	0.44 ± 0.29	69.36 ± 0.20	0.48 ± 0.40	67.32 ± 0.44	0.92 ± 0.69
	FA-GNN	59.78 ± 0.96	1.01 ± 1.29	69.57 ± 0.28	**2.58 ± 0.58**	67.26 ± 0.49	0.95 ± 0.42
	Gradient Ascent	65.19 ± 0.47	1.01 ± 1.29	69.21 ± 0.16	1.25 ± 0.43	-	-
	G-FairAttack	64.34 ± 0.45	**1.79 ± 1.30**	69.83 ± 0.14	2.30 ± 0.49	67.30 ± 0.47	**1.12 ± 1.04**
EDITS	Clean	70.95 ± 0.28	0.38 ± 0.00	70.89 ± 0.44	5.15 ± 0.51	69.11 ± 0.50	6.15 ± 1.67
	Random	68.13 ± 0.20	0.97 ± 0.68	70.89 ± 0.44	5.15 ± 0.51	69.04 ± 0.06	**6.93 ± 2.13**
	FA-GNN	70.72 ± 0.27	0.38 ± 0.00	70.89 ± 0.44	5.15 ± 0.51	69.11 ± 0.50	6.16 ± 1.66
	Gradient Ascent	68.36 ± 0.24	0.57 ± 0.56	70.89 ± 0.44	5.15 ± 0.51	-	-
	G-FairAttack	68.12 ± 0.22	**1.23 ± 0.73**	70.99 ± 0.44	**6.18 ± 1.23**	69.04 ± 0.06	**6.93 ± 2.13**

Table 7: Experiment results of fairness poisoning attack, where ACC and Δ_{dp} are adopted as the prediction utility metric and the fairness metric, correspondingly.

Victim	Attack	Facebook		Pokec_z		Credit	
		ACC(%)	Δ_{dp}(%)	ACC(%)	Δ_{dp}(%)	ACC(%)	Δ_{dp}(%)
GCN	Clean	80.25 ± 0.64	6.33 ± 0.54	61.51 ± 0.54	8.39 ± 1.25	69.77 ± 0.36	10.61 ± 0.73
	Random	80.15 ± 1.02	4.17 ± 1.58	60.98 ± 0.29	7.76 ± 0.93	69.71 ± 0.55	10.96 ± 1.35
	FA-GNN	79.41 ± 0.67	5.84 ± 0.32	59.97 ± 0.90	2.46 ± 1.18	69.56 ± 0.81	**18.58 ± 1.78**
	Metattack	79.30 ± 1.15	**33.33 ± 5.97**	60.14 ± 0.29	**44.90 ± 0.10**	-	-
	G-FairAttack	78.55 ± 0.18	14.99 ± 2.08	61.81 ± 0.21	6.15 ± 1.52	69.57 ± 1.13	10.87 ± 0.96
Reg	Clean	80.41 ± 0.18	4.63 ± 1.18	65.20 ± 1.26	1.55 ± 0.82	68.22 ± 0.73	1.48 ± 0.28
	Random	80.18 ± 0.30	1.41 ± 1.23	63.00 ± 1.50	2.01 ± 1.98	68.62 ± 0.48	1.58 ± 0.64
	FA-GNN	79.38 ± 0.31	1.42 ± 0.89	64.02 ± 0.47	0.76 ± 0.81	69.29 ± 0.63	0.79 ± 0.41
	Metattack	80.81 ± 0.40	9.45 ± 0.96	62.89 ± 1.90	4.88 ± 1.62	-	-
	G-FairAttack	77.95 ± 0.16	**15.65 ± 0.69**	65.45 ± 0.55	**7.76 ± 0.08**	67.80 ± 1.34	**2.32 ± 0.51**
FairGNN	Clean	80.36 ± 0.18	2.71 ± 0.50	60.87 ± 3.00	0.80 ± 0.62	75.57 ± 0.65	4.78 ± 1.58
	Random	78.66 ± 0.00	0.18 ± 0.31	54.21 ± 5.10	1.79 ± 0.93	75.42 ± 0.57	5.08 ± 1.71
	FA-GNN	78.77 ± 0.18	0.33 ± 0.58	60.54 ± 2.48	1.24 ± 0.77	75.38 ± 0.88	4.89 ± 0.56
	Metattack	78.66 ± 0.84	3.86 ± 3.51	55.16 ± 6.70	**6.08 ± 3.64**	-	-
	G-FairAttack	77.92 ± 0.18	**10.64 ± 0.97**	59.36 ± 1.19	3.91 ± 3.07	75.47 ± 0.56	**5.85 ± 1.66**
EDITS	Clean	79.62 ± 1.10	1.36 ± 1.54	62.33 ± 0.84	3.32 ± 0.64	67.73 ± 0.46	7.23 ± 0.33
	Random	81.21 ± 0.32	3.86 ± 2.27	62.49 ± 0.69	4.62 ± 0.97	69.19 ± 0.86	7.91 ± 0.91
	FA-GNN	79.83 ± 0.18	3.04 ± 0.50	63.38 ± 0.18	2.47 ± 1.38	67.55 ± 0.89	7.30 ± 0.19
	Metattack	81.95 ± 1.21	4.50 ± 0.67	62.72 ± 0.19	2.83 ± 0.80	-	-
	G-FairAttack	81.95 ± 0.48	**6.15 ± 0.77**	62.65 ± 0.81	**4.85 ± 0.44**	69.01 ± 0.79	**8.14 ± 0.41**

F.3 Attack Patterns

In this experiment, we compare the patterns of G-FairAttack with FA-GNN (Hussain et al., 2022). FA-GNN divides edges into four different groups, 'EE', 'ED', 'DE', and 'DD', where edges in EE link two nodes with the same label and the same sensitive attribute, edges in ED link two nodes with the same label and different sensitive attributes, edges in DE link two nodes with different labels and the same sensitive attribute, edges in DD link two nodes with different labels and different sensitive attributes In particular, we record the proportion of poisoned edges in these four groups yielded by

Table 8: Experiment results of fairness poisoning attack, where AUC and Δ_{eo} are adopted as the prediction utility metric and the fairness metric, correspondingly.

Victim	Attack	Facebook		Pokec_z		Credit	
		AUC(%)	Δ_{eo}(%)	AUC(%)	Δ_{eo}(%)	AUC(%)	Δ_{eo}(%)
GCN	Clean	64.53 ± 0.05	1.16 ± 0.78	67.53 ± 0.25	10.16 ± 1.20	69.36 ± 0.08	9.83 ± 0.76
	Random	65.49 ± 0.37	1.29 ± 0.87	66.97 ± 0.11	8.81 ± 1.07	69.45 ± 0.06	10.18 ± 1.62
	FA-GNN	64.45 ± 0.68	2.51 ± 0.33	65.77 ± 0.43	1.78 ± 0.66	69.16 ± 0.11	**18.55 ± 2.02**
	Metattack	65.02 ± 0.17	**24.84 ± 6.37**	64.33 ± 0.33	**43.71 ± 1.18**	-	-
	G-FairAttack	62.41 ± 0.07	9.53 ± 1.56	67.26 ± 0.26	9.71 ± 1.84	69.37 ± 0.14	10.23 ± 1.29
Reg	Clean	64.57 ± 0.21	1.02 ± 0.91	68.93 ± 1.25	1.39 ± 0.85	69.70 ± 0.49	1.01 ± 1.40
	Random	64.45 ± 0.36	1.40 ± 0.62	66.41 ± 2.23	1.22 ± 0.41	69.79 ± 0.46	0.86 ± 1.00
	FA-GNN	61.67 ± 0.53	0.29 ± 0.58	66.65 ± 0.66	3.05 ± 2.29	69.67 ± 0.76	1.42 ± 0.79
	Metattack	64.31 ± 0.17	4.88 ± 1.43	65.94 ± 2.99	6.23 ± 0.38	-	-
	G-FairAttack	61.69 ± 0.14	**9.80 ± 0.91**	68.06 ± 1.58	**6.88 ± 2.35**	69.76 ± 0.49	**2.36 ± 1.50**
FairGNN	Clean	65.57 ± 0.40	0.65 ± 0.78	65.22 ± 2.04	0.94 ± 0.83	65.95 ± 0.46	3.04 ± 1.35
	Random	64.66 ± 0.75	0.19 ± 0.33	59.56 ± 1.92	2.46 ± 2.43	65.48 ± 0.55	3.35 ± 1.41
	FA-GNN	63.54 ± 0.14	0.00 ± 0.00	64.73 ± 2.79	2.13 ± 1.35	65.13 ± 0.60	3.19 ± 0.66
	Metattack	65.10 ± 0.42	3.60 ± 4.13	57.99 ± 8.86	**7.13 ± 3.07**	-	-
	G-FairAttack	62.99 ± 0.29	**4.70 ± 1.44**	65.79 ± 2.64	2.78 ± 1.51	65.89 ± 0.53	**3.83 ± 1.64**
EDITS	Clean	79.00 ± 2.49	0.19 ± 0.33	67.00 ± 0.59	3.19 ± 0.84	69.83 ± 0.13	6.81 ± 0.49
	Random	71.58 ± 0.36	1.03 ± 0.95	68.23 ± 0.62	6.79 ± 1.00	69.55 ± 0.27	6.91 ± 1.05
	FA-GNN	77.06 ± 2.13	0.58 ± 0.58	67.55 ± 0.32	2.86 ± 2.67	69.82 ± 0.17	6.83 ± 0.52
	Metattack	71.60 ± 0.40	0.52 ± 0.44	67.51 ± 0.56	3.15 ± 1.23	-	-
	G-FairAttack	70.33 ± 1.76	**1.61 ± 0.59**	68.26 ± 0.57	**6.98 ± 0.29**	69.62 ± 0.20	**7.29 ± 0.53**

Table 10: Attack patterns (statistics of poisoned edges in different groups) of G-FairAttack.

Dataset	Fairness Evasion Attack				Fairness Poisoning Attack			
	EE/%	ED/%	DE/%	DD/%	EE/%	ED/%	DE/%	DD/%
Facebook	43.46	28.42	14.44	13.96	31.86	28.72	19.07	20.34
Pokec	25.51	23.47	26.39	24.63	26.58	24.73	22.01	26.68
Credit	74.89	7.37	16.06	1.68	38.63	22.59	24.78	13.99

G-FairAttack and FA-GNN. The results of attack patterns of G-FairAttack are shown in Table 10. According to the study in (Hussain et al., 2022), injecting edges in DD and EE can increase the statistical parity difference. Based on this guidance, FA-GNN randomly injects edges that belong to group DD to attack the fairness of GNNs. Hence, the attack patterns of FA-GNN for all datasets and attack settings are all the same, i.e., 100% for the DD group and 0% for the other groups. However, our proposed G-FairAttack has different patterns of poisoned edges. For the Facebook and the Credit dataset, G-FairAttack poisons more EE edges than other groups. For the Pokec dataset, the proportion of poisoned edges in four groups is balanced. Although we cannot analyze the reason for the apparent difference in this paper, we can argue that G-FairAttack is much harder to defend because it does not have a fixed pattern for all cases, unlike FA-GNN.

F.4 Attack Generalization

Although the generalization capability of adversarial attacks on GNNs with a linearized surrogate model has been verified by previous works (Zügner et al., 2018; Zügner & Günnemann, 2019), we conduct numerical experiments to verify the generalization capability of G-FairAttack to other GNN architectures. In the experiments, G-FairAttack is still trained with a two-layer linearized GCN as the surrogate model, while we choose two different GNN architectures, GraphSAGE (Hamilton et al., 2017) and GAT (Veličković et al., 2018), as the backbone of adopted victim models. Experimental results are shown in Tables 11 to 14. From the results, we can observe that G-FairAttack still successfully reduces the fairness of victim models with different GNN backbones, and G-FairAttack still has the most desirable performance on attacking different types of fairness-aware GNNs. In addition, to verify the generality of G-FairAttack, we conduct experiments on the German Credit dataset (Agarwal et al., 2021). In the German dataset, nodes represent customers of a German bank, and edges

Table 11: Experiment results of fairness evasion attack on the Facebook dataset. All victim models adopt GraphSAGE as the GNN backbone.

	Attack	ACC(%)	AUC(%)	Δ_{dp}(%)	Δ_{eo}(%)
SAGE	Clean	93.20 ± 0.15	93.78 ± 0.08	14.00 ± 0.72	7.08 ± 0.64
	Random	93.95 ± 0.26	94.32 ± 0.11	15.14 ± 0.63	7.21 ± 0.64
	FA-GNN	93.31 ± 0.26	93.83 ± 0.07	13.14 ± 0.63	5.28 ± 0.64
	Gradient Ascent	92.99 ± 0.26	94.00 ± 0.02	14.67 ± 0.63	$\mathbf{7.98 \pm 0.64}$
	G-FairAttack	93.42 ± 0.30	93.63 ± 0.09	$\mathbf{15.33 \pm 0.25}$	7.53 ± 0.00
Reg	Clean	91.93 ± 0.15	93.82 ± 0.12	4.13 ± 0.72	1.93 ± 0.27
	Random	92.78 ± 0.15	94.41 ± 0.13	$\mathbf{6.44 \pm 0.47}$	2.32 ± 0.00
	FA-GNN	92.04 ± 0.26	93.91 ± 0.05	2.95 ± 1.32	0.58 ± 0.27
	Gradient Ascent	91.83 ± 0.15	93.89 ± 0.10	3.67 ± 0.44	1.55 ± 0.55
	G-FairAttack	92.15 ± 0.30	93.72 ± 0.13	5.46 ± 0.25	$\mathbf{2.38 \pm 0.91}$
FairGNN	Clean	87.26 ± 0.94	93.74 ± 0.50	0.91 ± 0.56	0.90 ± 0.64
	Random	87.16 ± 0.91	93.83 ± 0.40	1.83 ± 1.13	0.45 ± 0.64
	FA-GNN	87.37 ± 1.17	93.07 ± 0.48	1.91 ± 1.06	0.45 ± 0.64
	Gradient Ascent	87.48 ± 0.84	93.58 ± 0.47	1.14 ± 0.63	$\mathbf{0.90 \pm 0.64}$
	G-FairAttack	87.26 ± 1.30	93.66 ± 0.48	$\mathbf{2.16 \pm 0.96}$	$\mathbf{0.90 \pm 0.64}$
EDITS	Clean	93.42 ± 0.15	93.62 ± 0.03	8.94 ± 0.41	1.22 ± 0.64
	Random	92.60 ± 0.14	93.82 ± 0.16	11.57 ± 0.20	$\mathbf{6.76 \pm 0.00}$
	FA-GNN	93.39 ± 0.14	93.67 ± 0.07	9.07 ± 0.42	1.45 ± 0.68
	Gradient Ascent	92.83 ± 0.27	93.80 ± 0.09	$\mathbf{12.29 \pm 0.63}$	5.75 ± 0.58
	G-FairAttack	92.57 ± 0.15	93.74 ± 0.12	11.61 ± 0.22	$\mathbf{6.76 \pm 0.00}$

Table 12: Experiment results of fairness poisoning attack on the Facebook dataset. All victim models adopt GraphSAGE as the GNN backbone.

	Attack	ACC(%)	AUC(%)	Δ_{dp}(%)	Δ_{eo}(%)
SAGE	Clean	91.83 ± 0.18	94.05 ± 0.11	16.78 ± 0.58	9.40 ± 0.78
	Random	92.99 ± 0.32	94.09 ± 0.03	15.91 ± 0.52	8.56 ± 0.45
	FA-GNN	93.10 ± 0.48	94.83 ± 0.10	11.09 ± 0.71	5.22 ± 0.00
	Metattack	92.15 ± 0.18	92.91 ± 0.15	$\mathbf{19.16 \pm 0.75}$	11.84 ± 0.99
	G-FairAttack	90.66 ± 0.18	93.83 ± 0.04	18.89 ± 0.27	$\mathbf{12.94 \pm 0.33}$
Reg	Clean	83.86 ± 0.48	93.08 ± 0.22	4.03 ± 0.53	0.45 ± 0.78
	Random	82.69 ± 0.37	93.24 ± 0.15	3.96 ± 0.31	0.00 ± 0.00
	FA-GNN	83.33 ± 0.37	93.06 ± 0.31	5.38 ± 0.54	0.00 ± 0.00
	Metattack	84.39 ± 0.00	92.58 ± 0.17	2.54 ± 0.00	0.00 ± 0.00
	G-FairAttack	84.50 ± 0.48	90.73 ± 0.37	$\mathbf{6.19 \pm 0.29}$	$\mathbf{2.70 \pm 0.00}$
FairGNN	Clean	88.96 ± 2.05	94.17 ± 0.19	2.54 ± 1.71	1.35 ± 0.00
	Random	86.73 ± 3.19	94.06 ± 0.33	2.89 ± 2.32	0.00 ± 0.00
	FA-GNN	86.09 ± 4.42	94.48 ± 0.23	1.61 ± 0.70	0.00 ± 0.00
	Metattack	86.41 ± 2.89	93.75 ± 0.15	3.13 ± 2.24	0.90 ± 0.78
	G-FairAttack	86.41 ± 0.80	92.90 ± 0.30	$\mathbf{5.03 \pm 0.48}$	$\mathbf{3.15 \pm 0.78}$
EDITS	Clean	91.08 ± 0.00	92.08 ± 0.28	4.57 ± 0.74	1.36 ± 0.33
	Random	92.25 ± 0.18	93.83 ± 0.09	16.74 ± 1.14	9.72 ± 1.26
	FA-GNN	89.17 ± 0.32	91.23 ± 0.17	5.46 ± 0.75	7.41 ± 1.45
	Metattack	91.83 ± 0.49	93.65 ± 0.11	17.27 ± 0.72	10.04 ± 0.89
	G-FairAttack	92.04 ± 0.32	93.55 ± 0.13	$\mathbf{17.58 \pm 0.47}$	$\mathbf{10.43 \pm 0.58}$

are generated based on the similarity between credit accounts. The task is to predict whether a customer has a high credit risk or low, with gender as the sensitive attribute. In this experiment, we choose GraphSAGE (Hamilton et al., 2017) as the backbone of the victim models and adopt both fairness evasion and poisoning settings. Experimental results are shown in Tables 16 and 17. We can observe that the superiority of G-FairAttack is preserved on the German dataset. In conclusion, supplementary experiments verify the generalization capability of G-FairAttack in attacking victim models with various GNN architectures and consolidate the universality of G-FairAttack.

Table 13: Experiment results of fairness evasion attack on the Facebook dataset. All victim models adopt GAT as the GNN backbone.

	Attack	ACC(%)	AUC(%)	Δ_{dp}(%)	Δ_{eo}(%)
	Clean	79.93 ± 1.39	66.97 ± 2.36	2.84 ± 1.34	0.71 ± 0.44
	Random	79.30 ± 0.55	67.33 ± 0.50	1.11 ± 0.47	0.51 ± 0.48
GAT	FA-GNN	80.15 ± 0.48	67.45 ± 2.45	**4.62 ± 1.60**	0.26 ± 0.44
	Gradient Ascent	80.25 ± 1.40	67.30 ± 2.16	4.24 ± 1.16	$\underline{1.35 \pm 1.00}$
	G-FairAttack	79.09 ± 1.21	66.76 ± 2.50	$\underline{4.35 \pm 1.66}$	**1.73 ± 1.67**
	Clean	80.15 ± 0.36	66.50 ± 1.08	4.88 ± 0.60	0.52 ± 0.48
	Random	79.83 ± 0.48	67.68 ± 1.29	2.82 ± 2.10	0.45 ± 0.49
Reg	FA-GNN	80.15 ± 0.36	69.79 ± 1.89	**5.64 ± 0.96**	**1.10 ± 0.95**
	Gradient Ascent	80.36 ± 0.18	65.89 ± 1.27	5.19 ± 1.22	0.52 ± 0.59
	G-FairAttack	78.77 ± 0.37	66.74 ± 1.09	$\underline{5.48 \pm 1.66}$	$\underline{1.09 \pm 0.29}$
	Clean	79.19 ± 0.67	66.17 ± 1.75	2.47 ± 2.94	0.64 ± 0.29
	Random	79.62 ± 0.55	62.54 ± 2.47	1.49 ± 0.84	0.26 ± 0.44
FairGNN	FA-GNN	79.19 ± 0.74	64.29 ± 3.51	1.84 ± 2.15	$\underline{0.90 \pm 0.62}$
	Gradient Ascent	78.98 ± 0.32	64.03 ± 1.73	$\underline{2.73 \pm 2.82}$	0.39 ± 0.33
	G-FairAttack	78.45 ± 0.80	63.94 ± 2.30	**3.69 ± 2.41**	**2.13 ± 0.78**
	Clean	79.30 ± 0.96	68.59 ± 3.81	0.66 ± 0.60	3.27 ± 2.19
	Random	76.01 ± 1.76	63.08 ± 1.90	$\underline{0.81 \pm 0.65}$	**4.74 ± 2.04**
EDITS	FA-GNN	79.30 ± 0.96	68.58 ± 3.87	0.66 ± 0.60	$\underline{3.27 \pm 2.19}$
	Gradient Ascent	77.50 ± 1.50	61.28 ± 2.44	$\underline{0.81 \pm 0.20}$	2.95 ± 3.62
	G-FairAttack	76.01 ± 1.94	63.08 ± 1.92	**1.04 ± 0.59**	**4.74 ± 2.61**

Table 14: Experiment results of fairness poisoning attack on the Facebook dataset. All victim models adopt GAT as the GNN backbone.

	Attack	ACC(%)	AUC(%)	Δ_{dp}(%)	Δ_{eo}(%)
	Clean	69.21 ± 0.80	60.03 ± 0.52	8.09 ± 3.17	4.34 ± 4.09
	Random	71.76 ± 0.48	57.17 ± 1.87	3.81 ± 3.36	4.23 ± 4.39
GAT	FA-GNN	80.68 ± 0.49	73.64 ± 1.66	2.97 ± 1.22	3.27 ± 2.33
	Metattack	69.11 ± 0.85	63.29 ± 1.80	**74.62 ± 3.79**	**70.30 ± 2.58**
	G-FairAttack	73.35 ± 1.33	57.36 ± 2.10	$\underline{9.85 \pm 1.62}$	$\underline{5.30 \pm 3.20}$
	Clean	79.09 ± 0.81	64.86 ± 0.81	2.22 ± 2.57	0.71 ± 0.11
	Random	78.98 ± 0.32	67.50 ± 0.53	1.00 ± 1.00	0.00 ± 0.00
Reg	FA-GNN	78.66 ± 0.00	69.19 ± 2.44	0.00 ± 0.00	0.00 ± 0.00
	Metattack	76.85 ± 1.29	63.39 ± 1.12	$\underline{8.60 \pm 7.05}$	**7.40 ± 5.04**
	G-FairAttack	78.77 ± 0.37	59.78 ± 1.00	**10.99 ± 1.47**	$\underline{7.28 \pm 0.99}$
	Clean	78.56 ± 0.48	56.57 ± 7.18	1.09 ± 1.50	0.77 ± 1.33
	Random	78.66 ± 1.15	52.88 ± 1.68	1.20 ± 0.69	1.15 ± 0.70
FairGNN	FA-GNN	77.17 ± 2.57	49.37 ± 4.58	$\underline{1.29 \pm 2.23}$	$\underline{1.23 \pm 2.12}$
	Metattack	79.30 ± 0.55	52.19 ± 4.20	0.62 ± 0.68	0.84 ± 1.13
	G-FairAttack	77.60 ± 0.97	57.90 ± 5.65	**3.20 ± 2.88**	**4.12 ± 3.65**
	Clean	73.89 ± 1.99	61.19 ± 3.47	4.36 ± 2.94	3.59 ± 4.22
	Random	78.88 ± 0.97	62.58 ± 3.75	1.83 ± 0.88	$\underline{3.02 \pm 1.12}$
EDITS	FA-GNN	78.66 ± 0.00	58.58 ± 3.62	0.00 ± 0.00	0.00 ± 0.00
	Metattack	78.77 ± 2.35	69.58 ± 5.19	$\underline{2.77 \pm 0.94}$	0.84 ± 0.77
	G-FairAttack	75.58 ± 5.61	64.60 ± 8.87	**6.96 ± 4.05**	**5.19 ± 7.07**

F.5 Advanced Attack Baselines

We supplement experiments on more previous attacks with fairness-targeted adaptations. We choose two more recent adversarial attacks for GNNs in terms of prediction utility, namely MinMax (Wu et al., 2019) and PRBCD (Geisler et al., 2021). To satisfy our fairness attack settings, we modify the attacker's objective with the demographic parity loss term (in the same way as adapting gradient ascent attack and Metattack). We implement all attack baselines in a fairness evasion attack setting with the same budget (5%). We compare the performance of these attacks with G-FairAttack based on four different victim models with GraphSAGE as the GNN backbone on the Facebook dataset. Results are shown in Table 15. From the experimental results, we can observe that (1) G-FairAttack

Table 15: Experiment results of fairness evasion attack on the Facebook dataset compared with more advanced attack baselines. All victim models adopt GraphSAGE as the GNN backbone.

	Attack	ACC(%)	AUC(%)	Δ_{dp}(%)	Δ_{eo}(%)	Train ACC(%)
SAGE	Clean	92.36 ± 0.32	94.06 ± 0.14	16.71 ± 0.79	10.10 ± 0.41	100.00 ± 0.00
	PRBCD	92.68 ± 0.00	94.26 ± 0.10	15.23 ± 0.31	8.11 ± 0.33	99.62 ± 0.00
	MinMax	92.99 ± 0.00	94.32 ± 0.15	$\underline{15.69 \pm 0.31}$	$\underline{8.69 \pm 0.33}$	98.66 ± 0.19
	G-FairAttack	92.15 ± 0.37	93.89 ± 0.15	**18.71 ± 0.74**	**11.91 ± 0.97**	100.00 ± 0.00
Reg	Clean	91.29 ± 0.49	93.69 ± 0.13	0.86 ± 0.83	1.79 ± 1.87	98.66 ± 0.33
	PRBCD	91.72 ± 0.85	94.00 ± 0.07	$\underline{1.33 \pm 2.00}$	$\underline{1.73 \pm 0.33}$	98.08 ± 0.51
	MinMax	91.61 ± 0.49	94.01 ± 0.08	0.77 ± 0.41	$\underline{1.73 \pm 0.33}$	97.19 ± 0.11
	G-FairAttack	91.19 ± 0.37	93.66 ± 0.12	**1.80 ± 0.60**	**2.12 ± 1.20**	98.53 ± 0.29
FairGNN	Clean	92.57 ± 0.48	93.97 ± 0.20	3.38 ± 1.44	2.02 ± 0.58	98.98 ± 0.55
	PRBCD	92.46 ± 0.26	94.03 ± 0.26	3.36 ± 1.05	$\underline{1.93 \pm 0.33}$	98.53 ± 0.29
	MinMax	92.67 ± 0.55	94.12 ± 0.27	$\underline{3.53 \pm 1.60}$	$\underline{1.93 \pm 0.33}$	97.57 ± 0.29
	G-FairAttack	92.57 ± 0.18	93.80 ± 0.23	**4.40 ± 1.14**	**2.05 ± 1.25**	98.98 ± 0.55
EDITS	Clean	93.42 ± 0.18	93.66 ± 0.07	9.12 ± 0.58	1.67 ± 0.78	98.34 ± 0.11
	PRBCD	93.10 ± 0.73	93.88 ± 0.14	$\underline{10.78 \pm 1.15}$	**5.41 ± 2.34**	97.89 ± 0.19
	MinMax	93.20 ± 0.37	93.88 ± 0.13	**10.94 ± 1.70**	$\underline{4.31 \pm 1.90}$	97.45 ± 0.29
	G-FairAttack	93.10 ± 0.15	93.88 ± 0.15	$\underline{10.78 \pm 1.15}$	**5.41 ± 2.34**	97.95 ± 0.22

Table 16: Experiment results of fairness evasion attack on the German dataset. All victim models adopt GraphSAGE as the GNN backbone.

	Attack	ACC(%)	AUC(%)	Δ_{dp}(%)	Δ_{eo}(%)
SAGE	Clean	58.80 ± 1.06	66.56 ± 0.98	58.02 ± 5.05	56.20 ± 5.76
	Random	58.80 ± 1.06	66.44 ± 1.02	56.32 ± 2.70	53.57 ± 3.01
	FA-GNN	59.60 ± 0.80	68.44 ± 0.96	55.18 ± 3.90	52.66 ± 4.88
	Gradient Ascent	58.13 ± 1.51	66.14 ± 1.00	**59.52 ± 4.58**	**57.99 ± 4.93**
	G-FairAttack	58.00 ± 1.74	65.75 ± 1.21	$\underline{58.73 \pm 4.81}$	$\underline{56.83 \pm 4.95}$
Reg	Clean	61.87 ± 2.41	61.40 ± 0.78	2.91 ± 2.28	4.34 ± 1.76
	Random	61.33 ± 2.01	61.44 ± 0.96	3.90 ± 1.35	5.18 ± 1.08
	FA-GNN	62.00 ± 3.02	61.79 ± 0.65	3.69 ± 2.11	$\underline{5.22 \pm 2.05}$
	Gradient Ascent	61.20 ± 2.40	60.53 ± 1.02	$\underline{3.97 \pm 4.17}$	4.62 ± 2.99
	G-FairAttack	61.33 ± 2.27	61.49 ± 1.44	**4.61 ± 3.49**	**6.65 ± 2.53**
FairGNN	Clean	64.40 ± 3.12	59.73 ± 3.99	4.26 ± 3.39	5.36 ± 2.32
	Random	64.53 ± 3.11	59.71 ± 3.83	4.61 ± 2.80	5.67 ± 3.63
	FA-GNN	64.67 ± 2.89	60.03 ± 4.06	4.40 ± 2.85	**5.95 ± 3.22**
	Gradient Ascent	64.80 ± 3.17	59.40 ± 4.62	$\underline{4.90 \pm 2.86}$	5.64 ± 2.35
	G-FairAttack	64.27 ± 2.89	59.66 ± 3.57	**5.46 ± 3.14**	$\underline{5.92 \pm 2.33}$
EDITS	Clean	68.27 ± 1.97	57.48 ± 2.13	2.17 ± 1.22	3.12 ± 1.77
	Random	68.13 ± 1.22	58.90 ± 1.62	**2.81 ± 2.14**	**3.41 ± 2.13**
	FA-GNN	68.27 ± 1.97	57.48 ± 2.14	2.17 ± 1.22	3.12 ± 1.77
	Gradient Ascent	68.13 ± 1.22	58.90 ± 1.62	**2.81 ± 2.14**	**3.41 ± 2.13**
	G-FairAttack	68.13 ± 1.22	58.90 ± 1.62	**2.81 ± 2.14**	**3.41 ± 2.13**

has the most desirable performance in attacking different types of (fairness-aware) victim models and (2) G-FairAttack best preserves the prediction utility of victim models over the training set. In conclusion, we obtain that our proposed surrogate loss and constrained optimization technique help G-FairAttack address the two proposed challenges of fairness attacks while a simple adaptation of previous attacks is not effective in solving these challenges.

G Defense Against Fairness Attacks of GNNs

In this paper, the purpose of investigating the fairness attack problem on GNNs is to highlight the vulnerability of GNNs on fairness and to inspire further research on the fairness defense of GNNs. Hence, we would like to discuss the defense against fairness attacks of GNNs. Considering the difficulty in fairness defense, this topic deserves a careful further study, and we only provide some simple insights on defending against fairness attacks of GNNs in this section.

Table 17: Experiment results of fairness poisoning attack on the German dataset. All victim models adopt GraphSAGE as the GNN backbone.

	Attack	ACC(%)	AUC(%)	Δ_{dp}(%)	Δ_{eo}(%)
SAGE	Clean	59.60 ± 1.06	63.87 ± 1.30	41.29 ± 7.36	36.94 ± 7.94
	Random	62.13 ± 1.97	65.48 ± 0.57	41.52 ± 8.40	38.34 ± 5.29
	FA-GNN	64.67 ± 1.01	71.22 ± 2.08	43.99 ± 0.63	42.79 ± 2.16
	Metattack	58.13 ± 3.63	64.03 ± 0.71	$\underline{46.31 \pm 3.22}$	$\mathbf{43.87 \pm 3.49}$
	G-FairAttack	63.87 ± 2.34	66.10 ± 1.68	$\mathbf{47.98 \pm 4.99}$	$\underline{43.56 \pm 5.48}$
Reg	Clean	58.00 ± 2.50	60.70 ± 2.35	0.80 ± 0.28	1.37 ± 1.55
	Random	60.13 ± 2.84	61.83 ± 1.25	$\underline{0.80 \pm 0.13}$	3.15 ± 2.83
	FA-GNN	60.80 ± 1.74	64.42 ± 0.64	0.72 ± 0.88	$\underline{4.83 \pm 1.37}$
	Metattack	58.67 ± 1.01	60.21 ± 0.25	0.42 ± 0.33	2.59 ± 0.52
	G-FairAttack	57.87 ± 3.72	60.42 ± 1.48	$\mathbf{3.38 \pm 1.86}$	$\mathbf{7.77 \pm 3.48}$
FairGNN	Clean	60.91 ± 2.58	62.15 ± 3.70	1.87 ± 1.93	1.48 ± 1.50
	Random	66.33 ± 2.98	63.76 ± 5.71	$\underline{4.50 \pm 3.57}$	$\underline{6.33 \pm 4.44}$
	FA-GNN	68.22 ± 3.36	63.07 ± 5.19	2.59 ± 2.73	1.86 ± 1.10
	Metattack	67.78 ± 4.92	63.04 ± 4.35	2.06 ± 2.09	1.98 ± 1.07
	G-FairAttack	65.34 ± 4.70	64.32 ± 6.83	$\mathbf{7.86 \pm 1.68}$	$\mathbf{10.64 \pm 2.54}$
EDITS	Clean	64.01 ± 1.83	65.59 ± 0.92	12.74 ± 1.44	6.66 ± 3.28
	Random	61.90 ± 1.16	66.18 ± 1.56	10.02 ± 3.78	7.84 ± 5.78
	FA-GNN	63.45 ± 2.51	64.66 ± 1.55	$\underline{19.45 \pm 2.53}$	$\underline{13.62 \pm 3.63}$
	Metattack	62.24 ± 0.51	63.46 ± 1.97	15.92 ± 8.11	10.77 ± 3.41
	G-FairAttack	65.34 ± 1.02	65.31 ± 1.49	$\mathbf{20.43 \pm 5.37}$	$\mathbf{15.30 \pm 5.53}$

(1). According to the study in (Hussain et al., 2022), injecting edges that belong to DD and EE groups can increase the statistical parity difference. Hence, a simple fairness defense strategy is to delete edges in DD and EE groups randomly. This strategy makes it possible to remove some poisoned edges in the input graph. However, this method cannot defend against G-FairAttack because G-FairAttack can poison the edges in all groups (EE, ED, DE, and DD).

(2). In our opinion, preprocessing debiasing frameworks such as EDITS can be a promising paradigm for fairness defense. Next, we explain the reasons in detail. We first review the processes of EDITS framework. EDITS is a preprocessing framework for GNNs (Dong et al., 2022a). First, we feed the clean graph into EDITS framework and obtain a debiased graph by reconnecting some edges and changing the node attributes where we can modify the debiasing extent with a threshold. Then, EDITS runs a vanilla GNN model (without fairness consideration), such as GCN, on the debiased graph. Finally, we find that the output of GCN on the debiased graph is less biased than the output of GCN on the clean graph. As a preprocessing framework, EDITS would flip the edges *again* to obtain a debiased graph for training *after* we poison the graph structure by attacking methods. Consequently, we can obtain that *EDITS can obtain very similar debiased graphs for any two different poisoned graphs with a strict debiasing threshold,* while the accuracy will also decrease as the debiasing threshold becomes stricter because the graph structure has been changed too much. In conclusion, EDITS has a tradeoff between the debiasing effect and the prediction utility. EDITS can be a strong fairness defense method for GNNs by sacrificing the prediction utility.

(3). A possible defense strategy against fairness attacks of GNNs is to solve a similar optimization problem as Problem 1 while minimizing the attacker's objective as

$$\begin{gathered}\min_{\mathbf{A}'\in\mathcal{F}} \mathcal{L}_f\left(g_{\boldsymbol{\theta}^*}, \mathbf{A}', \mathbf{X}, \mathcal{Y}, \mathcal{V}_{\text{test}}, \mathcal{S}\right) \\ s.t.\ \ \boldsymbol{\theta}^* = \arg\min_{\boldsymbol{\theta}} \mathcal{L}_s\left(g_{\boldsymbol{\theta}}, \mathbf{A}', \mathbf{X}, \mathcal{Y}, \mathcal{S}\right),\ \|\mathbf{A}' - \mathbf{A}\|_F \le 2\Delta, \\ \mathcal{L}(g_{\boldsymbol{\theta}^*}, \mathbf{A}, \mathbf{X}, \mathcal{Y}, \mathcal{V}_{\text{train}}) - \mathcal{L}(g_{\boldsymbol{\theta}^*}, \mathbf{A}', \mathbf{X}, \mathcal{Y}, \mathcal{V}_{\text{train}}) \le \epsilon.\end{gathered} \tag{17}$$

The meaning of this optimization problem is to find the rewired graph structure that minimizes the prediction bias. The prediction bias is computed based on the model trained on the rewired graph. It can be seen as an inverse process of G-FairAttack. As a result, we can rewire the problematic edges that hurt the fairness of the model trained on the rewired graph.

H BROADER IMPACT

Adversarial attacks on fairness can make a significant impact in real-world scenarios (Solans et al., 2021; Mehrabi et al., 2021; Hussain et al., 2022). In particular, fairness attacks can exist in many different real-world scenarios.

- For personal benefits, malicious attackers can exploit the fairness attack to affect a GNN model (for determining the salary of an employer or the credit/loan of a user account) into favoring specific demographic groups by predicting higher values of money while disadvantaging other groups.
- For commercial competitions, a malicious competitor can attack the fairness of a GNN-based recommender system deployed by a tech company and make its users unsatisfied, especially when defending techniques of GNNs' utility have been widely studied while defending techniques of GNNs' fairness remain undeveloped.
- For governmental credibility, malicious adversaries can attack models used by a government agency with the goal of making them appear unfair in order to depreciate their value and credibility.

In addition, adversarial attack on fairness is widely studied on independent and identically distributed data. Extensive works (Chang et al., 2020b; Solans et al., 2021; Mehrabi et al., 2021; Van et al., 2022; Chhabra et al., 2023) have verified the vulnerability of algorithmic fairness of machine learning models. In this paper, we find the vulnerability of algorithmic fairness also exists in GNNs by proposing a novel adversarial attack on fairness of GNNs. It has the potential risk of being leveraged by malicious attackers with access to the input data of a deployed GNN model. Despite that, our research has a larger positive influence compared with the potential risk. Considering the lack of defense methods on fairness of GNNs, our study highlights the vulnerability of GNNs in terms of fairness and inspires further research on the fairness defense of GNNs. Moreover, we also provide discussions on attack patterns and simple ways to defend against fairness attacks.